6678-6688.
Pushkin, J. S., & Martin, T. (1979) *Biochim. Biophys. Acta 552*, 53-65.
Rosenberg, J., Düzgünes, N., & Kayalar, C. (1983) *Biochim. Biophys. Acta 735*, 173-180.
Shaw, J. M., Hutton, W. C., Lentz, B. R., & Thompson, T. E. (1977) *Biochemistry 16*, 4156-4163.
Siegel, D. P. (1987) in *Cell Fusion* (Sowers, A. E., Ed.) pp 181-207, Plenum Publishing Corp., New York.
van Deenen, L. L. M. (1981) *FEBS Lett. 123*, 3-15.
Zachowski, A., Favre, E., Cribier, S., Hervé, P., & Devaux, P. F. (1986) *Biochemistry 25*, 2585-2690.

Analysis of Protein-Mediated 3-*O*-Methylglucose Transport in Rat Erythrocytes: Rejection of the Alternating Conformation Carrier Model for Sugar Transport†

Amy L. Helgerson and Anthony Carruthers*

Department of Biochemistry, University of Massachusetts Medical Center, 55 Lake Avenue North, Worcester, Massachusetts 01605

Received August 10, 1988; Revised Manuscript Received January 4, 1989

ABSTRACT: 3-*O*-Methylglucose (3OMG) transport in rat erythrocytes (RBCs) is mediated by a low-capacity, facilitated diffusion-type process. This study examines whether the characteristics of sugar transport in rat RBCs are consistent with the predictions of two diametric, theoretical mechanisms for sugar transport. The *one-site carrier* describes a transport mechanism in which sugar influx and efflux substrate binding sites are mutually exclusive. The *two-site carrier* describes a transport mechanism in which sugar influx and efflux substrate binding sites can exist simultaneously but may interact in a cooperative fashion when occupied by substrate. Michaelis and velocity parameters for saturable 3OMG transport in rat erythrocytes at 24 °C were obtained from initial rate measurements of 3OMG transport. The results are incompatible with the predictions of the one-site carrier but are consistent with the predictions of a symmetric two-site carrier, displaying negligible cooperativity between substrate binding sites. This allows reduction of the two-site carrier transport equations to a form containing fewer constants than the one-site carrier equations without limiting their predictive success. While the available evidence does not prove that rat erythrocyte sugar transport is mediated by a two-site mechanism, we conclude that adoption of the formally more complex one-site model for sugar transport in rat erythrocytes in unnecessary and unwarranted. Counterflow experiments have also been performed in which the time course of radiolabeled 3OMG uptake is measured in cells containing saturating levels of 3OMG. The results of these experiments are consistent with the hypothesis [Naftalin et al. (1985) *Biochim. Biophys. Acta 820*, 235-249] that exchange of sugar between intracellular compartments (cell water and hemoglobin) can be rate limiting for transport under certain conditions.

Passive, saturable sugar transport in eukaryotic cells is mediated by an integral membrane protein(s) of 42-60-kDa molecular mass (Mueckler et al., 1985; Birnbaum et al., 1986; Allard & Lienhard, 1985). While the functional and structural properties of sugar transport systems may display subtle species and tissue differences (e.g., in stereoselectivity for sugars, heterogeneity of transporter glycosylation, sensitivity to inhibitors, susceptibility to physiological regulation, etc.), the similarities between the systems studied to date [with the notable exception of hepatocyte transporter (Birnbaum et al., 1986) and the insulin-sensitive adipocyte carrier (James et al., 1988)] suggest both a common evolutionary origin and a common catalytic mechanism (Mueckler et al., 1985; Birnbaum et al., 1986).

The catalytic mechanism of sugar transport is the subject of some controversy. A variety of theoretical transport models have been proposed to account for the facilitated diffusion of D-glucose (DG)[1] across human red cell membranes. These include the classical asymmetric one-site (mobile or alternating conformer) carrier (Widdas, 1952; Regen & Tarpley, 1974), the asymmetric two-site (linear or simultaneous) carrier (Baker & Widdas, 1973), the tetramer model (Lieb & Stein, 1971), the allosteric pore model (Holman, 1980), the bi-antiparallel asymmetric one-site system (Ginsburg, 1978), the symmetric two-site carrier model rate limited by intracellular water and sugar complexation (Naftalin & Holman, 1977; Naftalin et al., 1985), and the two-site allosteric carrier model (Helgerson & Carruthers, 1987). Each of these models fails to account for some of the experimental properties of red cell sugar transport [for reviews of these and additional models, see Naftalin and Holman (1977) and Stein (1986)]. This has led a number of workers to propose that the apparent complexity of human erythrocyte hexose transfer results from technical problems associated with transport determinations rather than

† This work was supported by National Institutes of Health Grant RO1 AM36081.
* Author to whom correspondence should be addressed.

[1] Abbreviations: CCB, cytochalasin B; CCD, cytochalasin D; CCE, cytochalasin E; 3OMG, 3-*O*-methyl-α-D-glucopyranoside; DG, D-glucose; Hb, hemoglobin; P_{sat}, permeability coefficient for protein-mediated transport; K_L, rate constant for transmembrane sugar leakage; RBC, red blood cell.

0006-2960/89/0428-4580$01.50/0

from an inherent complexity of the transport process per se (Lowe & Walmsley, 1986, 1987; Naftalin et al., 1985; Wheeler, 1986).

A major difficulty in studying human erythrocyte hexose transfer arises from the unusually high density of plasmalemmal sugar transport proteins (Jung & Rampal, 1977). This complicates determinations of initial rates of transport at 20–37 °C, where hexose transfer is extremely rapid. Recent applications of rapid-quenching techniques permitting transport determinations over millisecond intervals (Lowe & Walmsley, 1986) have illustrated that many earlier studies may have overestimated $K_{m(app)}$ for DG exit from red cells (Carruthers & Melchior, 1983; Stein, 1986).

In this study we analyze the 3OMG transport properties of rat erythrocytes. Rat red cells contain 200–400-fold fewer sugar transport proteins than do human erythrocytes and thus allow estimates of initial rates of transport over intervals of minutes. The major advantage this affords is in the accuracy of timing, where errors in arresting transport by cells are minimized. The approach we take here is to ask: Is it possible to distinguish potential mechanisms for sugar transport with transport data alone? We test the ability of two transport models (the one-site and two-site allosteric carrier mechanisms) to predict the sugar transport properties of rat erythrocytes. Prevailing doctrine asserts that the least complex model should be adopted in situations where more than one model is successful (Lieb & Stein, 1974). We demonstrate by statistical analysis of experimental transport data that the predictions of the two-site allosteric carrier model provide a significantly better fit of experimental data than do the predictions of the one-site carrier model. In addition, we show that the two-site carrier model can be simplified to a form containing fewer constants than the one-site carrier model without limiting the predictive success of the model. We conclude that adoption of the formally more complex one-site carrier model for rat erythrocyte sugar transport is unwarranted.

Models for Sugar Transport

Definitions. See Chart I for definitions of subscripts and variables used.

The One-Site (Alternating Conformer) Carrier. This model describes a theoretical transport system in which the sugar carrier contains sugar binding sites for influx and efflux but where these sites are mutually exclusive. Thus at any instant, the carrier contains a sugar binding site exposed to either the extracellular or intracellular milieu but not to both environments. This model is shown in King–Altman form:

$$\begin{array}{ccc} X_2 + S_2 & \rightleftharpoons & X{\cdot}S_2 \\ \uparrow\downarrow & & \uparrow\downarrow \\ X_1 + S_1 & \rightleftharpoons & X{\cdot}S_1 \end{array}$$

where X_2 and X_1 refer to isomers of the carrier capable of binding either extracellular (S_2) or intracellular (S_1) sugar, respectively.

The steady-state equation for unidirectional efflux (v_{12}) via the one-site carrier model is characterized by five constants (three independent and one dependent resistance R_n terms and the intrinsic affinity constant K) and is given by Lieb and Stein (1974) and Stein (1986) as

$$\frac{-dN_1}{dt} = v_{12} = \frac{KS_1 + S_1S_2}{K^2R_{oo} + KR_{12}S_1 + KR_{21}S_2 + R_{ee}S_1S_2} \quad (1)$$

where N_1 is the amount of intracellular sugar S in 1 unit of red cells (that number of cells containing 1 L of water) and where

Chart I: Definitions of Subscripts and Variables

subscript 1	interior of the cell
subscript 2	exterior of the cell
superscript and subscript s	sugar species s
superscript and subscript p	sugar species p
S	concentration of sugar species s
P	concentration of sugar species p
V_{12}^{zt}	V_{max} for sugar efflux into sugar-free medium (zero-trans exit)
V_{21}^{zt}	V_{max} for sugar entry into sugar-free cells (zero-trans entry)
V^{ee}	V_{max} for sugar transport when intracellular [sugar] = extracellular [sugar] (equilibrium exchange)
K_{12}^{zt}	$K_{m(app)}$ for sugar efflux into sugar-free medium (zero-trans exit)
K_{21}^{zt}	$K_{m(app)}$ for sugar entry into sugar-free cells (zero-trans entry)
K^{ee}	$K_{m(app)}$ for sugar transport when intracellular [sugar] = extracellular [sugar] (equilibrium exchange)
K_{12}^{ic}	concentration of extracellular sugar reducing saturated net sugar efflux by half and, when $V^{ee} > V_{12}^{zt}$, concentration of extracellular sugar stimulating saturated unidirectional sugar efflux by half (infinite-cis exit)
K_{21}^{ic}	concentration of intracellular sugar reducing saturated net sugar uptake by half and, when $V^{ee} > V_{21}^{zt}$, concentration of intracellular sugar stimulating saturated unidirectional sugar entry by half (infinite-cis entry)
K_{12}^{it}	concentration of intracellular sugar at which unidirectional sugar efflux into medium containing saturating sugar is half-maximal (infinite-trans exit)
K_{21}^{it}	concentration of extracellular sugar at which unidirectional sugar influx into cells containing saturating sugar is half-maximal (infinite-trans entry)

$$V_{12}^{zt} = \frac{1}{R_{12}} \qquad K_{12}^{zt} = \frac{KR_{oo}}{R_{12}}$$

$$V_{21}^{zt} = \frac{1}{R_{21}} \qquad K_{21}^{zt} = \frac{KR_{oo}}{R_{21}}$$

$$V^{ee} = \frac{1}{R_{ee}} \qquad K^{ee} = \frac{KR_{oo}}{R_{ee}}$$

$$K_{12}^{ic} = \frac{KR_{12}}{R_{ee}} \qquad K_{21}^{ic} = \frac{KR_{21}}{R_{ee}}$$

Influx is obtained by interchanging subscripts 1 and 2. Under exchange efflux conditions the unidirectional efflux $-dN_1/dt$ is given by

$$v_{12}^{s} = \left(\frac{S_1}{K^s} + \frac{S_1S_2}{K^sK^s} + \frac{S_1P_2}{K^sP^p}\right) \Bigg/ \left(R_{oo} + R_{12}^{s}\frac{S_1}{K^s} + R_{21}^{s}\frac{S_2}{K^s} + R_{12}^{p}\frac{P_1}{K^p} + R_{21}^{p}\frac{P_2}{K^p} + R_{ee}^{s}\frac{S_1S_2}{K^sK^s} + R_{ee}^{sp}\frac{S_1P_2}{K^sK^p} + R_{ee}^{ps}\frac{P_1S_2}{K^pK^s} + R_{ee}^{p}\frac{P_1P_2}{K^pK^p}\right) \quad (2)$$

where R_{ee}^{s} is the reciprocal of V_{max} (V^{ee}) for equilibrium exchange S transport, R_{ee}^{p} is the reciprocal of V_{max} (V^{ee}) for equilibrium exchange P transport, R_{ee}^{sp} is the reciprocal of V_{max} (V_{sp}^{ee}) for equilibrium exchange efflux of S into extracellular

sugar P, and R_{ee}^{ps} is the reciprocal of V_{max} (V_{ps}^{ee}) for equilibrium exchange efflux of P into extracellular sugar S. K^p and K^s are the intrinsic affinity constants for sugars P and S, respectively. P and S could refer to DG and 3OMG, respectively (heteroexchange), or to 3-*O*-methylglucose and [^{14}C]-3-*O*-methylglucose, respectively. For extracellular DG (P) stimulation of 3OMG (S) exit, K^p and R_{21}^p can be determined from zero-trans entry of P, remembering that R_{oo} (which is independent of sugar type) is already determined from the transport data with S. Influx is obtained by interchanging subscripts 1 and 2. The heteroexchange infinite-cis unidirectional exit equation is thus characterized by six constants (K^s, K^p, R_{oo}, R_{12}^s, R_{21}^p, and R_{ee}^{sp}).

For the homoexchange counterflow experiment (i.e., S is [^{14}C]-3OMG and P is 3OMG), Stein (1986) shows that at the peak of the counterflow transient where the rate of radiolabel exit is identical with the rate of radiolabel entry

$$K = \frac{P_1 - (S_1/S_2)P_2}{(S_1/S_2) - 1} \tag{3}$$

where S_1/S_2 is the ratio of [^{14}C]-3OMG inside:[^{14}C]-3OMG outside and P_1 and P_2 are the concentrations of 3OMG inside and ouside the cell, respectively. This procedure thus permits the determination of K under conditions where initial rate estimates are not necessary.

The Two-Site Carrier. This theoretical carrier is distinguished from the one-site carrier in that two sugar molecules (one at the influx and the other at the efflux site) can bind to the carrier simultaneously. The two-site carrier is shown in its simplest form; i.e., we assume rapid equilibrium kinetics:

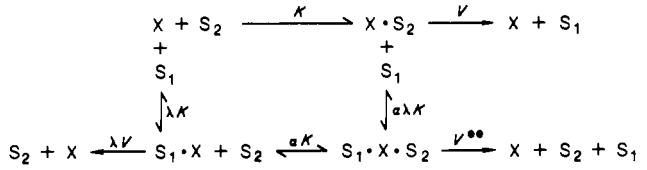

Assuming rapid equilibrium kinetics (Baker & Widdas, 1973; Helgerson & Carruthers, 1987), unidirectional sugar efflux (v_{12}) is characterized by five constants and is given by

$$v_{12} = \frac{\lambda V\frac{S_1}{\lambda K} + V^{ee}\frac{S_1S_2}{\alpha\lambda K^2}}{1 + \frac{S_1}{\lambda K} + \frac{S_2}{K} + \frac{S_1S_2}{\alpha\lambda K^2}} \tag{4}$$

λ represents the degree of asymmetry in transport and α the cooperativity between binding sites. λK and K for sugar S are $K_{m(app)}$ for zero-trans exit and entry, respectively, and λV and V^{ee} are V_{max} for zero-trans exit and equilibrium exchange. Influx is obtained by interchanging subscript 1 and 2, λK and K, and V and λV. The constants α and λ are obtained as

$$\alpha = \frac{K_{12}^{ic}}{K_{21}^{zt}} = \frac{K_{21}^{ic}}{K_{12}^{zt}} \qquad \lambda = \frac{V_{12}^{zt}}{V_{21}^{zt}} = \frac{K_{12}^{zt}}{K_{21}^{zt}}$$

The heteroexchange condition (S efflux into sugar P) is obtained in the following fashion. K represents $K_{m(app)}$ for zero-trans entry of sugar S. K^p represents $K_{m(app)}$ for zero-trans entry of sugar P, and V_{sp}^{ee} is V_{max} for saturated S_1 exit into saturating levels of P_2. The heteroexchange exit equation is obtained by interchanging K and K^p, V^{ee} and V_{sp}^{ee}, and S_2 and P_2, resulting in an equation characterized by six constants (λ, V, K^s, K^p, V_{sp}^{ee}, and α).

Under homocounterflow conditions (S is [^{14}C]-3OMG and P is unlabeled 3OMG), uptake of S is given by

$$v_{21} = \frac{V\frac{S_2}{K} + V^{ee}\frac{S_2(S_1 + P_1)}{\alpha\lambda K^2}}{1 + \frac{S_1 + P_1}{\lambda K} + \frac{S_2 + P_2}{K} + \frac{(S_1 + P_1)(S_2 + P_2)}{\alpha\lambda K^2}} \tag{5}$$

and exit of S is given by interchanging subscripts 1 and 2 and λV and λK for V and K in the numerator. The asymmetry between Michaelis and velocity parameters for exit and entry, λ, can be estimated from the peak of the homoexchange counterflow transient where radiolabel influx is identical with radiolabel exit. Here, it can be shown that

$$\lambda = \frac{V^{ee}}{\alpha VK}\frac{S_2P_1 - S_1P_2}{S_1 - S_2} \tag{6}$$

where P_1 and P_2 are the concentrations of 3OMG inside and outside the cell and S_1 and S_2 are the concentrations of intracellular and extracellular [^{14}C]-3OMG at the counterflow transient turning point.

Individual Procedures in Two-Site Transport. Here we consider transport via the two-site carrier in a simplified case where $\alpha = \lambda = 1$ (no cooperativity or asymmetry in transport).

(*A*) *Zero Trans.* Here S_1 is varied, $S_2 = 0$, and sugar flux is measured in the direction $1 \rightarrow 2$ or vice versa. Equation 4 reduces to the standard Michaelis–Menten form. Zero-trans exit (v_{12}) is given by

$$v_{12} = \frac{VS_1}{K + S_1} \tag{7}$$

Entry (v_{21}) is obtained by interchanging subscripts 1 and 2.

(*B*) *Infinite Trans Unidirectional.* Here eq 4 reduces to the standard Michaelis–Menten form. Infinite-trans exit describes a condition in which S_2 is saturating and S_1 is varied. Flux in the direction $1 \rightarrow 2$ (v_{12}) is given by

$$v_{12} = \frac{V_{app}S_1}{K + S_1} \tag{8}$$

where

$$V_{app} = \frac{V(K + \beta S_2)}{K + S_2} \qquad \beta = \frac{V^{ee}}{V}$$

V_{app} is independent of the varied substrate S_1. Entry is obtained by interchanging subscripts 1 and 2.

(*C*) *Infinite Cis Unidirectional.* Here eq 4 reduces to Michaelis–Menten kinetics. Infinite-cis exit describes a condition in which S_1 is saturating and S_2 is varied. Flux in the direction $1 \rightarrow 2$ (v_{12}) is given by

$$v_{12} = \frac{V_{app}S_1}{K + S_1} \tag{9}$$

where

$$V_{app} = \frac{V(K + \beta S_2)}{K + S_2}$$

V_{app} is independent of S_1. Here, saturated S_1 exit is half-maximally stimulated by S_2 when $S_2 = K_{0.5}$ and

$$v_{12} = \frac{V^{ee} - V_{12}^{zt}}{2} = \frac{\beta V - V}{2} = \frac{V(K + \beta S_2)}{K + S_2} - V$$

Thus

$$\beta + \frac{K}{S_2}(1 - \beta) = 1 \qquad \frac{K}{S_2} = 1$$

Thus saturated exit is half-maximally stimulated by S_2 when $S_2 = K_{0.5} = K$. Entry is obtained by interchanging subscripts 1 and 2.

(*D*) *Equilibrium Exchange Unidirectional.* Here eq 9 applies. In this condition under homoexchange conditions $S_1 = S_2 = S$, and uptake or exit (v^{ee}) is given by

$$v^{ee} = \frac{V^{ee}_{app} S}{K_{app} + S} \tag{10}$$

where

$$V^{ee}_{app} = \frac{V(K + \beta S)}{2K + S} \qquad K_{app} = \frac{K^2}{2K + S}$$

In this instance both V^{ee}_{app} and K_{app} are dependent upon the varied substrate S thus no discreet solution is available for these parameters. V^{ee}_{app} increases with S, and K_{app} falls with S. At any concentration of substrate, the ratio $V^{ee}_{app}/K_{app} = V/K + S(V^{ee}/K^2)$. Equilibrium exchange is half-maximal when $S = K_{0.5}$ and

$$\frac{V\beta}{2} = \frac{V^{ee}_{app} S}{K_{app} + S}$$

and thus

$$2K\left(1 - \frac{1}{\beta}\right) + \frac{K^2}{S} - S = 0 \tag{11}$$

Estimating and Predicting Michaelis and Velocity Parameters. This analysis is a two-part analysis. First, we estimate $K_{m(app)}$ and V_{max} for transport from the experimental data. We then calculate the various one- and two-site parameters from these data and use these parameters to predict the properties of one- and two-site carrier transport. Comparisons of experimental and predicted $K_{m(app)}$ and V_{max} parameters for each transport procedure permit detection of potential internal inconsistencies.

One-site carrier mediated transport obeys simple Michaelis–Menten kinetics under all conditions employed in this study. The various one-site constants (K and resistance terms) are obtained by Hanes–Woolf analysis of velocity/substrate concentration data assuming Michaelis–Menten kinetics (Table I). R_{oo} is calculated from the relationship $R_{oo} = R_{12} + R_{21} - R_{ee}$. These calculations then permit estimation of K. By use of estimated K and R parameters, $K_{m(app)}$ and V_{max} for the various transport conditions can then be predicted.

Two-site carrier mediated transport obeys simple Michaelis–Menten kinetics for all conditions other than equilibrium exchange. α, V, λV, K, and λK parameters can be estimated from zero-trans experimental data in an analogous fashion to the analysis of one-site carrier parameters (Table I).

Two-Site Carrier Equilibrium Exchange. No discreet solution for $K_{m(app)}$ and V_{max} exists for the equilibrium exchange condition over a range of [S]. In the simplest case ($\alpha = 1$), it is possible to both predict (see eq 11—knowing K, V, and β from zero-trans and infinite-trans and infinite-cis experiments) and to extrapolate (from experimental data) $K_{0.5}$—that concentration of 3OMG at which transport is half-maximal. Equation 11 can be solved for [3OMG] according to the Newton–Raphson procedure (Ralston & Rabinowitz, 1978). It is also possible to obtain estimates of K, β, and V from equilibrium exchange transport data with the Marquardt–Levenberg algorithm for nonlinear parameter estimation (Marquardt, 1963) in order to obtain a direct, best fit of eq 5 or 10 to the experimental transport data. These estimates of K, V, and β can then be compared with those determined experimentally in the zero- and infinite-trans procedures and infinite-cis procedure.

Thus working with either one- or two-site carrier models, the various transport constants may be derived experimentally and then employed to predict $K_{m(app)}$ and V_{max} parameters for the various experimental procedures. In this way, internal consistencies and inconsistencies may become apparent.

Simulating Counterflow Experiments. Our approach was similar to that of Naftalin et al. (1985). The system was considered to consist of three compartments: C_1^b contains the bulk intracellular sugar, C_1^m lies below the membrane and contains sugars that can readily access transport sites, and C_2 is the extracellular compartment. Exchange of sugar, J, between compartments C_1^b and C_1^m is described by the permeability coefficient D_1:

$$^{NET}J_{C_1^m \rightarrow C_1^b} = D_1\{S_{C_1^m} - S_{C_1^b}\} \tag{12}$$

Prior to injection of sugar-loaded cells into sugar-poor medium, the concentration of intracellular sugar in compartments C_1^b and C_1^m is identical although the amount of sugar present in each compartment (N^m and N^b) of a unit number of cells is proportional to compartment size. For simplicity, we consider the dead volume of the cell to be negligible (although this assumption is probably invalid) and that water flow between compartments is not restricted. Upon injection of cells into sugar-poor medium an osmotic water movement into the cell occurs. The concentration of S within compartment C_1^m (S^m) is given by

$$S_m = \frac{N_s^m}{V_r^m} \tag{13}$$

and the concentration of P in this compartment by

$$P^m = \frac{N_p^m}{V_r^m} \tag{14}$$

where V_r^m is the volume of compartment C_1^m relative to that under isotonic conditions. If Q is the osmolarity of osmotically active but nontransported species present in compartments C_2, C_1^b, and C_1^m under isotonic conditions and S_2 is the concentration of labeled sugar and P_2 the concentration of unlabeled sugar at the sugar-poor exterior of the cell, we have at osmotic equilibrium

$$Q + S_2 + P_2 = \frac{Q + N_s^m + N_p^m}{V_r^m} \tag{15}$$

giving

$$S^m = \frac{N_s^m(Q + S_2 + P_2)}{Q + N_s^m + N_p^m} \qquad P^m = \frac{N_p^m(Q + S_2 + P_2)}{Q + N_s^m + N_p^m} \tag{16}$$

and in analogous fashion for sugar in compartment C_1^b

$$S^b = \frac{N_s^b(Q + S^m + P^m)}{Q + N_s^b + N_p^b} \qquad P^b = \frac{N_p^b(Q + S^m + P^m)}{Q + N_s^b + N_p^b} \tag{17}$$

Numerical solutions to the differential exchange equations (one and two site; eq 2 and 5, respectively) allowing for transmembrane sugar leakage (K_L, see Results) and sugar exchange between intracellular compartments (eq 12) with correction for volume changes (eq 16 and 17) were obtained with fourth-order Runge–Kutta numerical integration using a Macintosh II computer and the software package Stella (High Performance Systems, Lyme, NH). We assigned a value of Q of 310 mosM, employed one-site carrier K and R values and

two-site K, V, V^{ee}, λ, and α values calculated from initial data (Tables II–IV), and arbitrarily varied the isotonic volumes of compartments C_I^b and C_I^m in an attempt to mimic the experimental findings. Step sizes (dt) employed in simulations were reduced until further reduction was without significant effect on the computed results.

Detecting Unstirred Layers Inside the Cell. Lieb and Stein (1974) demonstrate an analysis of zero-trans sugar exit in the special case where an unstirred layer exists within but not outside the cell. A Hanes–Woolf plot of initial rate data (S/v versus S) shows significant deviation from linearity at low values of S in the presence of an unstirred layer below the endofacial surface of the membrane. The permeability coefficient for S flux through this barrier (D_1) is obtained as 1/(experimental intercept − extrapolated intercept from data points at high S).

Materials and Methods

Materials. Sugars, cytochalasins, and phloretin were purchased from Sigma Chemicals. [^{3}H]Cytochalasin B, [^{14}C]inulin, [^{14}C]-3OMG, and [^{14}C]DG were purchased from New England Nuclear. Lactate and pyruvate assay kits were purchased from Sigma Chemicals. Cytochalasin stock solutions were made in dimethyl sulfoxide. Phloretin stock solutions were made in ethanol. Control solutions lacking CCB or phloretin contained the appropriate ethanol or dimethyl sulfoxide concentration. Dimethyl sulfoxide and ethanol concentrations never exceeded 0.1%.

Solutions. Saline consisted of 150 mM NaCl, 2 mM EDTA, and 5 mM Tris-HCl, pH 7.4. Lysis medium consisted of 10 mM Tris-HCl and 0.2 mM EDTA, pH 8. Tris medium consisted of 50 mM Tris-HCl, pH 7.4. All [^{3}H]cytochalasin B solutions were made in Tris medium. Stopping solution contained 224 mM NaCl, 5 mM Tris-HCl, 20 μM cytochalasin B, 50 μM phloretin, 2 μM $HgCl_2$, and 1.5 mM KI, pH 7.4 (0–2 °C).

Preparation of Erythrocytes. Male rats (100 g) were sacrificed by cervical dislocation, and blood was collected into saline by decapitation. Whole blood in saline was filtered through cheesecloth and washed by repeated centrifugation (15 min at 20000g) in saline. Following each centrifugation, the supernatant and buffy coat were removed by aspiration, and the red cell pellet was resuspended in saline. The red cell pellet was nominally free of white cells and platelets following three centrifugation/wash cycles. Washed red cells obtained from rats were resuspended in 100 volumes of saline and placed at 37 °C for 2 h. The cells were then incubated overnight at 4 °C. This procedure reduces intracellular DG to less than 20 μM prior to transport assays. Rat erythrocyte ghosts were prepared as described previously for human erythrocyte ghosts (Carruthers & Melchior, 1983).

Cytochalasin B Binding Experiments. The binding of [^{3}H]cytochalasin B to rat erythrocyte ghosts was measured as described previously (Helgerson & Carruthers, 1987) for human erythrocyte ghosts. The cytocrit of the final suspension of ghosts in [^{3}H]cytochalasin B solution was 33%. Binding consisted of at least three saturable components as detected by Scatchard analysis (Figure 1). These are site I, $K_{d(app)}$ = 100 nM, 800 sites per cell; site II, $K_{d(app)}$ = 50 nM, 1×10^4 sites per cell; and site III, $K_{d(app)}$ = 38 nM, 2.3×10^3 sites per cell. Cytochalasin D (at 10 μM), an agent with low affinity for the sugar transport system (see Results), completely blocked [^{3}H]cytochalasin B binding to site II. DG (500 mM) and/or phloretin (50 μM) but not mannitol or L-glucose (500 mM) abolished [^{3}H]cytochalasin B binding to site I but not to site III.

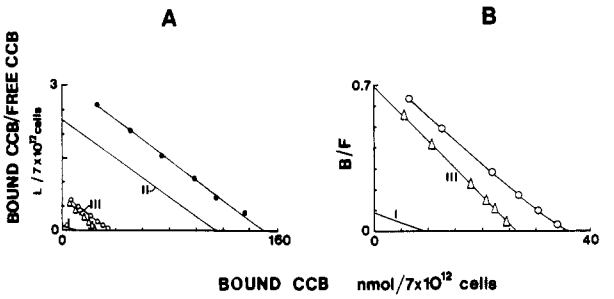

FIGURE 1: Equilibrium [^{3}H]cytochalasin B binding to rat erythrocyte ghosts. (A) Ordinate: bound/free cytochalasin B in moles of cytochalasin B per 7×10^{12} ghosts per mole of cytochalasin B per liter. Abscissa: bound cytochalasin B in nanomoles per 7×10^{12} ghosts. The various points represent averages of duplicate estimates of total binding (●), binding in the presence of 10 μM cytochalasin D (○), and binding in the presence of 10 μM cytochalasin D plus 500 mM DG (△). The cytochalasin D inhibitable component of binding is shown as site II, the DG inhibitable component as site I, and the DG cytochalasin D insensitive component as site III. Curve decompositions were obtained with an iterative procedure by computer (Helgerson & Carruthers, 1987). (B) Figure 2A expanded to show binding to sites I and III. Temperature of binding assays, 4 °C. $K_{d(app)}$ for binding to site I is given by $K_{d(app)} = K_{d(CCB)}\{1 + [CCD]/K_{d(CCD)}\}$, where $K_{d(CCD)}$ is $K_{i(app)}$ for cytochalasin D inhibition of sugar transport (125 μM; see Figure 4). The calculated slope for the site I plot obtained by the method of least squares is -0.0092 ± 0.0004 nM^{-1}; thus, $K_{d(CCB)}$ = 100.6 ■ 4.6 nM cytochalasin B.

Fate of Intracellular Glucose. Preliminary experiments indicated that rat erythrocytes metabolize DG but not 3-*O*-methylglucose. Cellular lactate and pyruvate levels could be maintained over 6 h by incubation of rat RBCs with DG but not with 3-*O*-methylglucose. In addition, tracer studies demonstrated that up to 15% of the intracellular ^{14}C in rat RBCs incubated with 50 μM [^{14}C]DG for 3 h was precipitable as sugar phosphates (Baker & Carruthers, 1981). Intracellular ^{14}C recovered from cells incubated with [^{14}C]-3-*O*-methylglucose for an equivalent period was not precipitable as sugar phosphates and upon paper chromatography (Helgerson & Carruthers, 1987) was identified as [^{14}C]-3-*O*-methylglucose. For this reason, efflux experiments in rat erythrocytes were performed with 3-*O*-methylglucose.

Estimation of Red Cell Water Content. Rat erythrocyte free and total water content and cell volume were estimated by three methods. Cells (20 μL) were equilibrated with 0.1 mM [^{14}C]-3OMG (1 mL) by incubation at 37 °C for 3 h. Equilibration is complete following 2-h incubation at this temperature. Following equilibration, the 3OMG space of the cells was estimated by counting the perchloric acid (1 mL, 3%) extract of cells submitted to two cycles of centrifugation in 10 mL of ice-cold stopping solution (to remove >99.99% extracellular activity). Total cellular water was estimated by measuring the wet and dry weight of 400-μL aliquots of packed cells. Cells were dried by vacuum drying (110 °C) for 2 h. Extracellular water contamination was calculated as the pelleted [^{14}C]inulin space of the packed cell aliquot (≈10–20%). Red blood cell volume was estimated by determining the hematocrit of cell suspensions of known amounts of cells by centrifugation in hematocrit tubes. Red cells were counted on a Coulter Counter. Using these procedures, we estimate rat red cell volume and water content as 66.4 ± 1.2 fL and 42.75 ± 1.3 fL, respectively.

Analytical. Protein assays were by the method of Lowry et al. (1951). Rat RBC and RBC ghost protein contents are 13.7 ± 0.9 pg and 0.4 ± 0.05 pg per cell, respectively.

Sugar Transport Determinations. Sugar transport was determined under zero-trans influx and efflux conditions, equilibrium exchange conditions, unidirectional infinite-cis

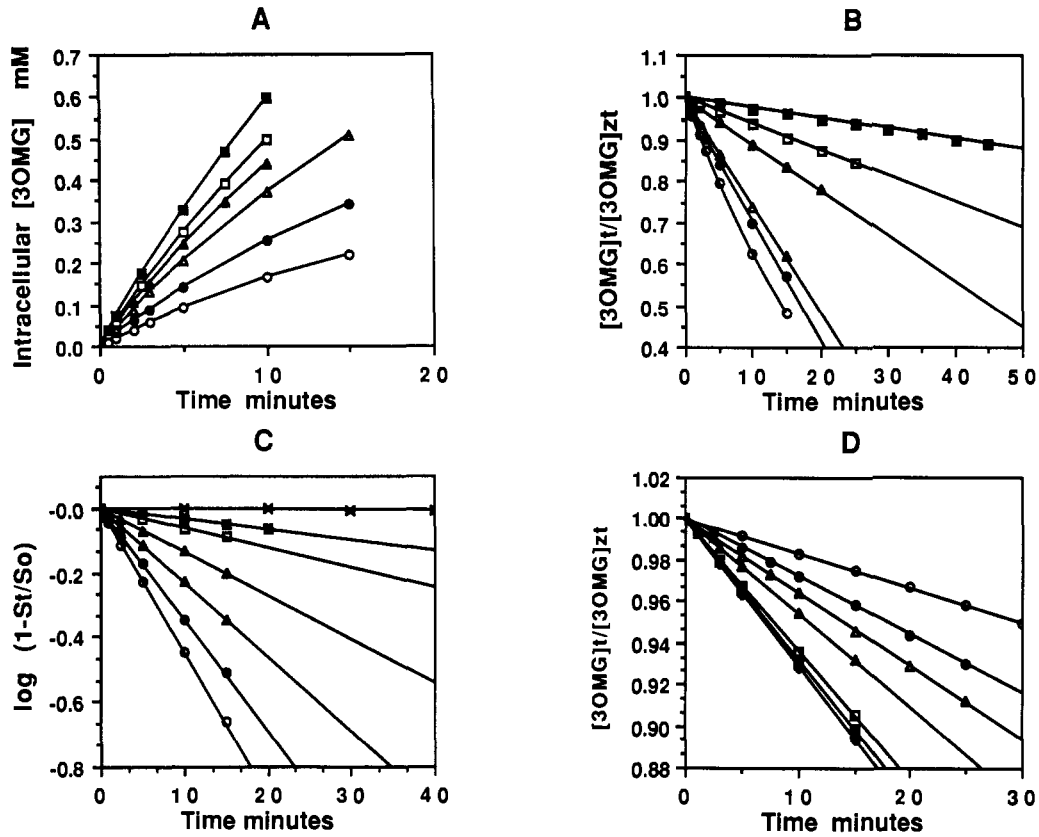

FIGURE 2: Time course of 3OMG transport in rat erythrocytes. (A) Zero-trans uptake. Ordinate: [$3OMG_i$] in millimolar. Abscissa: time in minutes. 3OMG uptake was measured at 0.5 (open circles), 1 (filled circles), 2.5 (open triangles), 5 (filled triangles), 10 (open squares), and 30 (filled squares) mM $3OMG_o$ (lowest to uppermost curves, progressively). Curves drawn by eye. (B) Zero-trans exit. Ordinate: [$3OMG_i$] when transport was arrested/[$3OMG_i$] at zero time. Abscissa: as in (A). The concentrations of $3OMG_i$ at zero time were 0.5, 1, 2.5, 5, 10, and 30 mM [same symbols as in (A)]. The curves (with the exception of exit at 0.5 mM) were calculated by the method of least squares. (C) Equilibrium-exchange 3OMG uptake. Ordinate: log $(1 - S_t/S_o)$, where S_t = [[^{14}C]-$3OMG_i$] at time t and S_o = [[^{14}C]-$3OMG_i$] at equilibrium and/or [[^{14}C]-$3OMG_o$]. Abscissa: as in (A). Uptake was measured at 1 (open circles), 2.5 (filled circles), 5 (open triangles), 10 (filled triangles), 25 (open squares), and 50 (filled squares) mM $3OMG_i$ = [$3OMG_o$] and at 50 mM 3OMG + 20 μM CCB + 50 μM phloretin (crosses) (lowest to uppermost curves, progressively). The lines drawn through the points were calculated by the method of least squares. (D) Infinite-cis unidirectional 3OMG exit. Ordinate: as in (B). Abscissa: as in (B). Initial [$3OMG_i$] = 50 mM. Extracellular [3OMG] = 0 (open circles), 0.25 (filled circles), 0.5 (open triangles), 1 (closed triangles), 5 (open squares), 10 (filled squares), 25 (open inverted triangles), and 50 (filled inverted triangles) mM (uppermost to lowest curves, progressively). Lines drawn through the points were calculated by the method of least squares. The data points in these experiments (A–D) represent the mean of duplicate measurements of a single experiment.

influx and efflux conditions, net infinite-cis exit conditions, and counterflow conditions (Naftalin & Holman, 1977).

General. Sugar transport determinations were made at 24 °C. The general protocol for all transport measurements was the following. Zero-time uptake points were obtained by immediately mixing cells with label and stopping medium. Zero-time exit points were obtained by mixing sugar-loaded cells with saline and stopper. The cells were then sedimented by centrifugation, resuspended in stopper, and sedimented a second time. For uptake measurements the cell pellet was counted. For exit experiments both the cell pellet and supernatant were counted. Time points were obtained by allowing the reaction to proceed for a specific time; then the reaction was arrested by addition of stopper. Equilibrium time points were obtained by incubation overnight at 37 °C. Uptake time points were corrected by subtraction of zero-time "uptake" and normalized relative to equilibrium uptake. Efflux time points were corrected by subtraction of extracellular zero-time label and normalized to equilibrium exit.

Time Courses. DG uptake at subsaturating levels (0.1 mM) at 24 °C is a linear function in time over the course of 0–15 min (half-time, $T_{1/2}$, for apparent equilibration at 24 °C is approximately 2.5 h, k = 0.0044 min^{-1}). Transport was therefore arrested at 10 min to obtain a measure of the initial rate of transport. Our analyses indicate that a substantial portion of DG penetrating the cells is metabolized to form sugar phosphates. DG efflux experiments are, therefore, technically unfeasible, and a detailed analysis of sugar transport in rat erythrocytes requires the use of a nonmetabolized but transported sugar—e.g., 3-*O*-methyl-α-D-glucopyranoside (3OMG).

The time course of 3OMG (0.5 mM) uptake by rat RBCs at 24 °C is apparently linear over the time interval 0–2 min with $T_{1/2}$ for uptake of 15–20 min (Figure 2A). $T_{1/2}$ for uptake and exit increases with [3OMG]. The strategy employed for analysis of initial rates of 3OMG uptake and exit was, therefore, to employ 0.2–5-min incubation periods at all [3OMG]. For estimates of leakage of sugars across the red cell membrane, transport was measured in the presence of saturating concentrations of cytochalasin B or phloretin or both cytochalasin B and phloretin. These agents are potent inhibitors of transport in rat erythrocytes (see Results). As leakage rates are low and are a linear function in [sugar] (see below), we monitored the time course of inhibited sugar uptake or exit over 0–60 min as a function of sugar concentration and then obtained an equilibrium point by overnight incubation at 37 °C. At this time, no additional uptake of 3OMG is detectable, and the 3OMG space of the cells (44.7 ± 2.6 fL/cell) is identical with that measured in the absence of transport inhibitors (43.4 ± 1.4 fL/cell). The rate constant for leakage at each sugar concentration employed was then obtained as the product [−2.3(slope)] from plots of log (1 −

S_t/S_∞) versus time for uptake and as the product [−2.3(slope)] from plots of log (S_t/S_0) versus time for exit, where S_0 is the amount of sugar in cells at zero time, S_t represents the amount of sugar in cells at time t, and S_∞ the amount of sugar in cells at equilibrium.

Zero-Trans Uptake. Uptake medium (500 μL containing cold and labeled sugar) was added to red cells (10 μL, 80–90% hematocrit), and the suspension was incubated at room temperature (24 °C) for the appropriate interval. During this period samples were taken for total counts and cell numbers. Following the appropriate incubation period, 10 mL of stopping solution was added to the cells. The cells were centrifuged lightly (4000*g* for 5 min, 4 °C), the supermatant was aspirated, and the wash/centrifugation cycle was repeated. The red cell pellet was extracted in 1 mL of 3% perchloric acid and centrifuged, and samples of the clear supernatant were counted in duplicate. Zero-time uptake measurements were made by simultaneously adding uptake medium and stopping solution to 10 μL of cells. These cells were processed as above, and the measured activity was subtracted from the counts associated with cells exposed to uptake medium for longer intervals. For 3OMG, equilibrium uptake points were obtained by incubation overnight at 37 °C in capped tubes by which time additional incubations demonstrated no further uptake of sugar.

Control experiments (additional 5-min centrifugations) indicated that sugar transport and leakage were arrested by ice-cold stopping solution and that loss of intracellular label was less than 3%. Results obtained by this procedure were indistinguishable from those obtained by spinning cells through oil (Hydol) for 30 s—a procedure that omits the wash/centrifugation cycles.

Zero-Trans 3OMG Efflux. Cells were loaded with the appropriate 3OMG concentration plus [^{14}C]-3OMG by incubation at 37 °C for 1–5 h. Equilibration of the intracellular space with external 3OMG was complete at these times—preliminary estimates indicating that V_{max} for 3OMG uptake is increased 3.5-fold over uptake at 24 °C at this temperature. The cells were then centrifuged, the supernatant was aspirated, and the cells were placed on ice. Cells (10 μL, 80–90% hematocrit) were aliquoted into tubes prewarmed to 24 °C and dispersed in 10 mL of saline (24 °C). Under these conditions, the extracellular sugar transport sites [$K_{m(app)} \approx 1$ mM] are never more than 1% saturated with sugar at zero time. Samples were taken for cell numbers. Following incubation for an appropriate time interval, 0.5 mL of suspension was sampled, transport was arrested by addition of 10 mL of stopper, the cells were pelleted by centrifugation, samples of the supernatant were counted, and the cells were processed as described above. This allows determination of exit rates by monitoring the loss of intracellular sugar and increase in extracellular sugar. During incubation, duplicate total samples were taken for counting. Zero-time counts were also taken by immediately sampling cells upon addition of saline followed by addition of 10 mL of stopping solution. Equilibrium time points were obtained as described for zero-trans entry. Figure 2B illustrates a time course experiment for 3OMG exit at varying initial [$3OMG_i$].

Equilibrium Exchange 3OMG Uptake. Cells were first loaded at 37 °C with unlabeled 3OMG as described above. Packed cells (10 μL) were aliquoted into tubes, and 10 mL of saline containing [^{14}C]-3OMG plus unlabeled 3OMG (at a concentration identical with that of loaded cells) was added to the cells. Totals were sampled, and transport was arrested at appropriate time intervals as described above. In theory, uptake of labeled 3OMG in equilibrium exchange experiments follows an exponential time course consisting of a leakage component characterized by rate constant k_L and a saturable or protein-mediated component characterized by rate constant k_{sat}. By plotting log ($1 - S_t/S_\infty$) versus time, a curve is obtained consisting of two linear components of slopes $-k_L/2.3$ and $-k_{sat}/2.3$, respectively. In practice, k_L is small, and the resulting plots appear linear at each [$3OMG_o$] (Figure 2C). k_L can be estimated directly from log plots of uptake in the presence of 50 μM CCB (where k_{sat} over the [3OMG] range 0.1–50 mM is reduced by more than 95%) versus time and the contribution of leakage to uptake subtracted from total uptake to calculate k_{sat}. k_L and k_{sat} were calculated from log plots of uptake by the method of least squares. Control experiments indicate that calculated $K_{m(app)}$ and V_{max} parameters for 3OMG equilibrium-exchange entry are indistinguishable from those for equilibrium-exchange exit.

Heteroexchange DG equilibrium exchange uptake was measured as described above for 3OMG, but here the extracellular sugar was DG and the intracellular sugar 3OMG.

Infinite-Cis Unidirectional Uptakes and Exits. These procedures were identical with those described for zero-trans fluxes with the following exceptions. (1) In influx experiments, the cells were first loaded with 0–50 mM unlabeled 3OMG, and the external 3OMG level was fixed at 50 mM plus [^{14}C]-3OMG. (2) In efflux experiments, the cells were loaded with 50 mM 3OMG plus [^{14}C]-3OMG, and the external unlabeled 3OMG or DG levels varied from 0 to 50 mM. Figure 2D illustrates some representative time course data for rat erythrocyte infinite-cis unidirectional 3OMG exit.

Infinite-Cis Net Exit. This procedure is identical with that described for unidirectional infinite-cis exit with the single exception that following loading with labeled 3OMG exit was monitored into varying levels of labeled 3OMG. The extracellular [^{14}C]-3OMG was of identical specific activity with that of the intracellular sugar and was obtained by dilution of the loading solution.

Counterflow Procedure. This two-part experiment in which the time course of 3.2 μM [^{14}C]-3OMG (in 1 mM unlabeled 3OMG) entry into unlabeled 3OMG-loaded (18–20 mM) cells at 24 °C is monitored was performed exactly as described by Naftalin et al. (1985).

Calculation of Michaelis and Velocity Constants for Transport. Under conditions where steady-state (initial) velocities were obtained as a function of sugar concentration, $K_{m(app)}$ and V_{max} for transport were calculated as in Table I. Unless stated otherwise V_{max} and $K_{m(app)}$ parameters listed in this study represent mean ±1 SD of $K_{m(app)}$ and V_{max} estimates from at least three separate experiments.

Results

Components and Inhibitors of Rat Erythrocyte Sugar Transport. The sugars DG and 3OMG penetrate rat erythrocytes by two functional routes—a saturable, cytochalasin B inhibitable pathway and a cytochalasin B insensitive, nonsaturable route. Figure 3A illustrates the DG concentration dependence of the initial rate of DG uptake by rat red cells in the presence and absence of 20 μM cytochalasin B. Uptake is significantly reduced by cytochalasin B and in the presence of the inhibitor is a linear function in [DG]. Defining saturable uptake as total uptake minus uptake in the presence of cytochalasin B, the mean (±1 SD) $K_{m(app)}$ for saturable DG uptake obtained from nonlinear regression analysis of four separate experiments is 6.8 ± 0.4 mM, and V_{max} is 30 ± 2 μmol (L of intracellular water)$^{-1}$ min^{-1}. Figure 3B illustrates that phloretin inhibits 3OMG efflux from rat erythrocytes. In the

Table I: Hanes–Woolf Analysis of Transport Data[a]

	one-site transport[b]		two-site transport[c]	
	x intercept	slope	x intercept	slope
zero trans				
entry	$-K_{21}^{zt}$	R_{21}	$-K$	$1/V$
exit	$-K_{12}^{zt}$	R_{12}	$-\lambda K\ (-K)^{d,e}$	$1/\lambda V\ (1/V)^{e}$
infinite cis[f]				
entry	$-K_{21}^{ic}$	R_{∞}	$-\alpha\lambda K\ (-K)^{d}$	$1/V^{\infty}$
exit	$-K_{12}^{ic}$	R_{∞}	$-\alpha K\ (-K)^{d}$	$1/V^{\infty}$
equilibrium exchange				
entry and exit	$-K^{\infty}$	R_{∞}	g	g

[a] The Hanes–Woolf analysis plots $[S]/v$ versus $[S]$, where $[S]$ is the substrate concentration and v is the initial rate of reaction at $[S]$. For systems obeying simple Michaelis–Menten kinetics the points fall on a single straight line with slope = $1/V_{max}$ and x intercept = $-K_{m(app)}$. [b] Interpretation of analysis for a one-site carrier mechanism. [c] Interpretation of analysis for a two-site carrier mechanism. [d] Interpretation if α and λ are unity. [e] Interpretation if λ is unity. [f] Data are plotted in the form $[S]/(v^{ic} - v^{zt})$ versus $[S]$, where $v^{ic} - v^{zt}$ is the increment in unidirectional transport produced by trans sugar over that observed in the absence of trans sugar (v^{zt}). [g] Not applicable here.

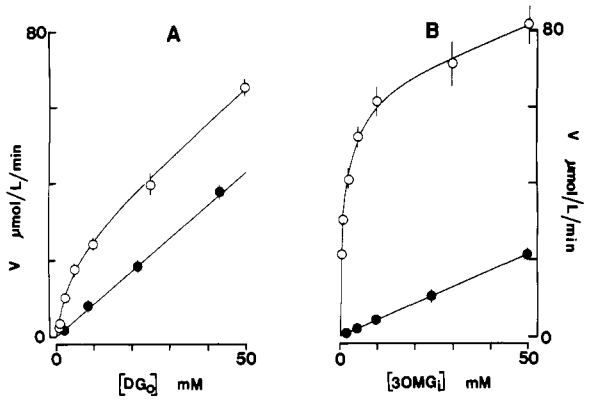

FIGURE 3: Sugar uptake and efflux from rat erythrocytes. (A) Dependence of the initial rate of DG uptake on DG concentration. Ordinate: sugar uptake rate in μmol (L of cell water)$^{-1}$ min^{-1}. Abscissa: [D-glucose] in mM. Uptake is shown in the absence (○) and presence (●) of 20 μM cytochalasin B. In the presence of cytochalasin B, uptake is described by the relationship, v [uptake in mmol (L of cell water)$^{-1}$ min^{-1}] = K_L[DG], where K_L was calculated by linear regression (shown by the straight line drawn through the points) as 0.0009 ± 0.00003 min^{-1}. In the absence of cytochalasin B, uptake is described by the linear component described in the presence of cytochalasin B plus a saturable component with $K_{m(app)}$ of 6.8 ± 0.4 mM and V_{max} of 30 ± 2 μmol L^{-1} min^{-1}. Each point consists of four or more separate duplicate determinations shown as mean ± SD. (B) Dependence of the initial rate of 3OMG exit on intracellular 3-*O*-methylglucose concentration. Ordinate: sugar exit rate in μmol (L of cell water)$^{-1}$ min^{-1}. Abscissa: [3OMG$_i$] in mM. Exit is shown in the absence (○) and presence (●) of 50 μM phloretin. In the presence of phloretin, exit is described by the relationship, v (exit in μmol (L of cell water)$^{-1}$ min^{-1}) = K_L[3OMG], where K_L was calculated by linear regression (shown by the straight line drawn through the points) as (4.4 ± 0.3) × 10^{-4} min^{-1}. In the absence of phloretin, exit is described by the linear component described in the presence of phloretin plus a saturable component with $K_{m(app)}$ of 0.9 ± 0.1 mM and V_{max} of 65 ± 8 μmol L^{-1} min^{-1}. Each point consists of triplicate determinations shown as mean ± SD.

presence of phloretin, efflux is a linear function in [3OMG$_i$] with k_L of 0.44 × 10^{-3} min^{-1}. In this experiment and in the absence of inhibitor, exit consists of a saturable component [$K_{m(app)}$ = 0.9 ± 0.1 mM; V_{max} = 65 ± 8 μmol (L of intracellular water)$^{-1}$ min^{-1} plus the noninhibitable component of exit. Zero-trans uptake of 3OMG in the presence of 20 μM CCB is a linear function in [3OMG] with k_L of 0.4 × 10^{-3} min^{-1} (not shown). This suggests that the rate of transmembrane 3OMG leakage is independent of the species of transport inhibitor employed and shows little rectification.

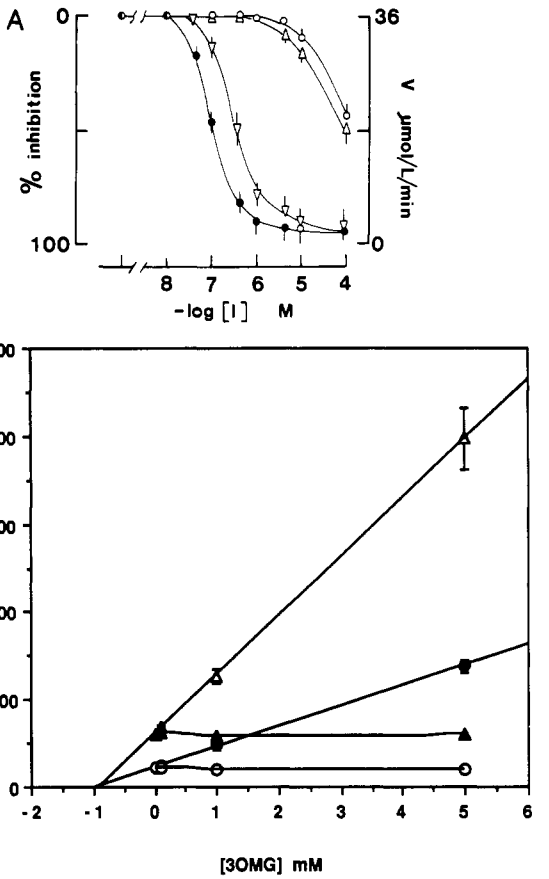

FIGURE 4: (A) Inhibition of 3-*O*-methylglucose exit by phloretin (inverted triangles) and DG uptake by cytochalasins B (filled circles), D (open circles), and E (triangles). Ordinate: inhibition of initial rates of entry and exit (%) and rate of 3OMG exit in μmol L^{-1} min^{-1}. Abscissa: log [inhibitor] (M). Uptake and exit were measured in triplicate at 1 mM sugar. The curves drawn through the points are inhibition of exit by phloretin, $K_{i(app)}$ = 0.31 ± 0.02 μM, maximum inhibition = 87 ± 6%; inhibition of entry by cytochalasin B, $K_{i(app)}$ = 0.11 ± 0.02 μM, maximum inhibition = 96.4 ± 2.8%; inhibitions of uptake by cytochalasins D and E (assuming 96% maximum inhibition), $K_{i(app)}$ = 125 ± 11 and 87 ± 18 μM, respectively. Points are shown as mean ± SD (for inhibition) of at least three determinations. (B) Effects of intracellular and extracellular [3OMG] on $K_{i(app)}$ for CCB and phloretin inhibition of sugar transport. The initial rate of either 3OMG exit or entry at varying [3OMG] (0.1–5 mM) was measured over a range of [CCB] or [phloretin] (0–50 μM). $K_{i(app)}$ for inhibition of transport was obtained as $-x$ intercept from linear regression analysis of plots of [I]/inhibition of transport versus [I], where I represents the inhibitor CCB or phloretin. The results are plotted in the form $K_{i(app)}$ versus [3OMG]. The circles represent studies in which CCB was the transport inhibitor and the triangles studies in which phloretin was the transport inhibitor. Filled and open symbols indicate zero-trans efflux and influx experiments, respectively. $K_{i(app)}$ for CCB and phloretin inhibition of transport are unaffected by increasing extracellular and intracellular 3OMG, respectively, but increase with increasing intra- and extracellular sugar, respectively. The lines drawn through the points for $K_{i(app)}$ for inhibition of exit by CCB and entry by phloretin were calculated by the method of least squares and in theory extrapolate to $-K_{m(app)}$ for 3OMG exit and entry, respectively, on the x axis. Leakage-mediated sugar fluxes (estimated as influx in the presence of 50 μM CCB and exit in the presence of 50 μM phloretin) were subtracted from total fluxes to obtain "saturable" transport. The results are shown as mean ± 1 SD of three duplicate estimates.

The concentration dependence of inhibition of sugar efflux by phloretin and sugar uptake by cytochalasins B, D, and E is shown in Figure 4A. Figure 4B summarizes the effects of intracellular and extracellular sugar on the $K_{i(app)}$ for inhibitions of sugar transport by phloretin and cytochalasin B.

Table II: Michaelis and Velocity Parameters for 3-*O*-Methylglucose Transport in Rat Erythrocytes[a]

procedure	$K_{m(app)}$[b]	V_{max}[c]
zero-trans entry	0.9 ± 0.07	64.7 ± 2.2
zero-trans exit	0.94 ± 0.06	64.2 ± 1.6
equilibrium exchange	2.5 ± 0.1[d]	386 ± 5
	2.2 ± 0.2[d,e]	
infinite-cis net exit	0.91 ± 0.08	65.5 ± 4
unidirectional infinite-cis exit	1.1 ± 0.2	379 ± 11
	8.5 ± 1.2[f]	373 ± 9[f]
unidirectional infinite-cis entry	0.9 ± 0.1	366 ± 15

[a] Michaelis and velocity paramaters were obtained from experimental data by Hanes–Woolf analysis assuming Michaelis–Menten kinetics. In all cases R^2 for the regression fit is >0.96. The number of experiments per condition was three or more with at least six substrate concentrations per procedure. V_{max} and $K_{m(app)}$ parameters were obtained from at least three separate experiments. These values were then averaged and are shown as mean ± 1 SD. [b] In mM. [c] In μmol (L of cell water)$^{-1}$ min^{-1}. [d] [3OMG] range = 0.5–50 mM. [e] Indicates the sugar concentration (mM) at which equilibrium exchange transport rates reach half-maximum ($K_{0.5}$). These values were obtained by first fitting the substrate/velocity data to a curve by interpolation (Stineman, 1980), followed by linear extrapolation of that point on the curve where $v = \beta V/2$ to the substrate axis. [f] In these experiments, the intracellular sugar was 50 mM 3OMG and the extracellular sugar was DG.

Extracellular sugar (but not intracellular sugar) increases $K_{i(app)}$ for phloretin inhibition of transport whereas intracellular sugar (but not extracellular sugar) increases $K_{i(app)}$ for cytochalasin B inhibition of transport.

Stereospecificity of Rat Erythrocyte Sugar Transport. A variety of sugars have been tested for their ability to compete with radiolabeled 3OMG for uptake in the rat erythrocyte. $K_{i(app)}$ for sugar inhibition of [^{14}C]-3OMG (3.2 μM) uptake was determined by Hanes–Woolf analysis. The order of potency of inhibition of uptake is 2-deoxy-D-glucose [$K_{i(app)}$ = 0.46 ± 0.02 mM] > 3-*O*-methylglucose [$K_{i(app)}$ = 1.07 ± 0.07 mM] > D-glucose [$K_{i(app)}$ = 6.8 ± 0.8 mM] > galactose [$K_{i(app)}$ = 9.6 ± 0.8 mM] ≫ maltose = methyl glucopyranoside = L-glucose = mannitol = no detectable inhibition at [sugar] ≤ 50 mM; five sugar concentrations were employed in duplicate in three separate experiments in all cases.

Kinetics of Rat Erythrocyte 3-O-Methylglucose Transport. A number of types of transport determinations are required to fully characterize the sugar transport mechanism of a cell (Stein, 1986). These experiments and the results are summarized in Table II. The most striking feature of rat erythrocyte sugar transport is the phenomenon of trans acceleration of transport—the stimulation of unidirectional sugar transport by the presence of sugar at the opposite, trans side of the membrane. Both DG and 3OMG uptake are stimulated by intracellular 3-*O*-methylglucose, and 3OMG exit is stimulated by extracellular 3OMG and DG. Trans acceleration is illustrated (Figures 2 and 5) for unidirectional infinite-cis 3OMG exit into 3OMG or DG.

Are Intra- and Extracellular Unstirred Layers Present? Lieb and Stein (1974) demonstrate a simple method for detecting the presence of unstirred layers inside or outside the cell. The initial rate of transport is determined over a wide range of sugar levels and then graphically represented in the form S^b/v or P^b/v versus S^b or P^b, where the superscript refers to the bulk solution concentration of S or P. At high P or S, the data fall on a single straight line with slope $1/V_{max}$, while at low P or S, if a significant cis-unstirred layer exists (inside and outside the cell for exit and uptake experiments, respectively), the data points deviate upward from the fit obtained from the data points at higher P or S. This is illustrated in Figure 6 for zero-trans 3OMG exit data. The exit data are

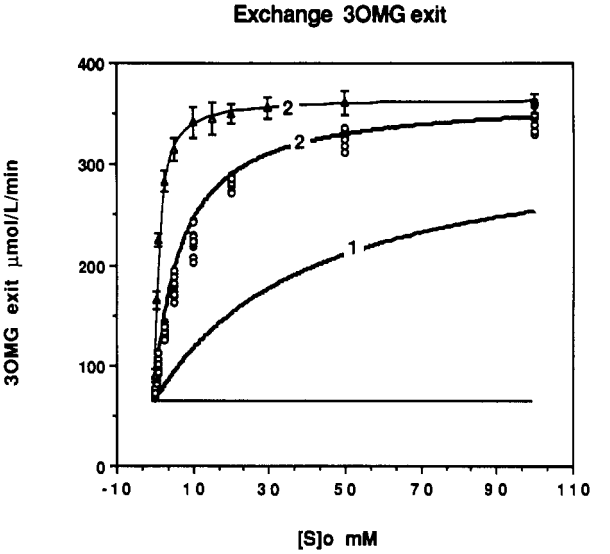

FIGURE 5: Trans acceleration of infinite-cis, unidirectional 3-*O*-methylglucose exit by extracellular sugars. 3OMG exit from cells containing 50 mM 3OMG was monitored into unlabeled DG (○) or 3OMG (△). Ordinate: initial rate of sugar exit in μmol L^{-1} min^{-1}. Abscissa: extracellular 3-*O*-methylglucose (△) or DG (○) level, in mM. The curve drawn through the 3OMG data points represents the predictions of the two-site carrier model for transport using K, V, β, λ, and α parameters of 0.94 mM, 64 μmol L^{-1} min^{-1}, 5.8, 1, and 1, respectively. Two curves are shown for the DG data points. Curve 1 (below the points) represents the predictions of the one-site carrier using zero-trans K and R parameters listed in Table III. Curve 2 (running close to the data points) represents the predictions of the two-site carrier with K of 6.8 mM and V of 30 μmol L^{-1} min^{-1} for zero-trans DG entry. These curves are superimposed upon base-line exit seen in the absence of extracellular sugar (shown by the line running parallel to the abscissa). Phloretin-insensitive zero-trans 3OMG exit has been subtracted from the data. Each 3OMG data point represents the mean ± SD of at least three separate duplicate determinations. The DG data points represent individual points from five separate experiments made in duplicate. They are shown in this form to demonstrate the scatter among determinations.

linear over the [3OMG] range 1–50 mM but deviate from a single straight line over the [3OMG] range 6.7–500 μM. This deviation at low [3OMG] exceeds the computed 95% confidence interval for the extrapolation of data at higher [3OMG]. This suggests the presence of an unstirred layer inside the cell. The equivalent uptake experiments showed no deviation from linearity at low [3OMG$_o$] (not shown). The permeability coefficient (D_i) for 3OMG flux across this intracellular barrier parallel to the membrane is obtained as the reciprocal of the difference between the extrapolated y intercept (calculated from the higher S_i^b levels) and the observed intercept. In this experiment D_i is 0.025 min^{-1} or 20 × 10^{-9} cm/s.

Counterflow Experiments. The counterflow experiment is a procedure in which cells are first loaded with relatively high sugar (3OMG) levels and the time course of uptake of radiolabeled sugar from medium containing low sugar levels is followed. Initially, a rapid counterflow transient is observed during which an apparent uphill movement of radiolabeled sugar is coupled to the net exit of intracellular sugar. Cellular radiolabel content reaches a maximum and then declines until the specific activity of sugar within the cell is identical with that in the extracellular medium. Two features account for the rapid accumulation of label in the cell. (1) Uptake is accelerated by the presence of sugar on the opposite site of the membrane. (2) High levels of unlabeled sugar within the cell compete with labeled sugar entering the cell for efflux, thus reducing the rate of labeled sugar efflux.

Figure 7 summarizes the results of five separate experiments in which the time course of uptake of [^{14}C]-3OMG (S_2, 3.2

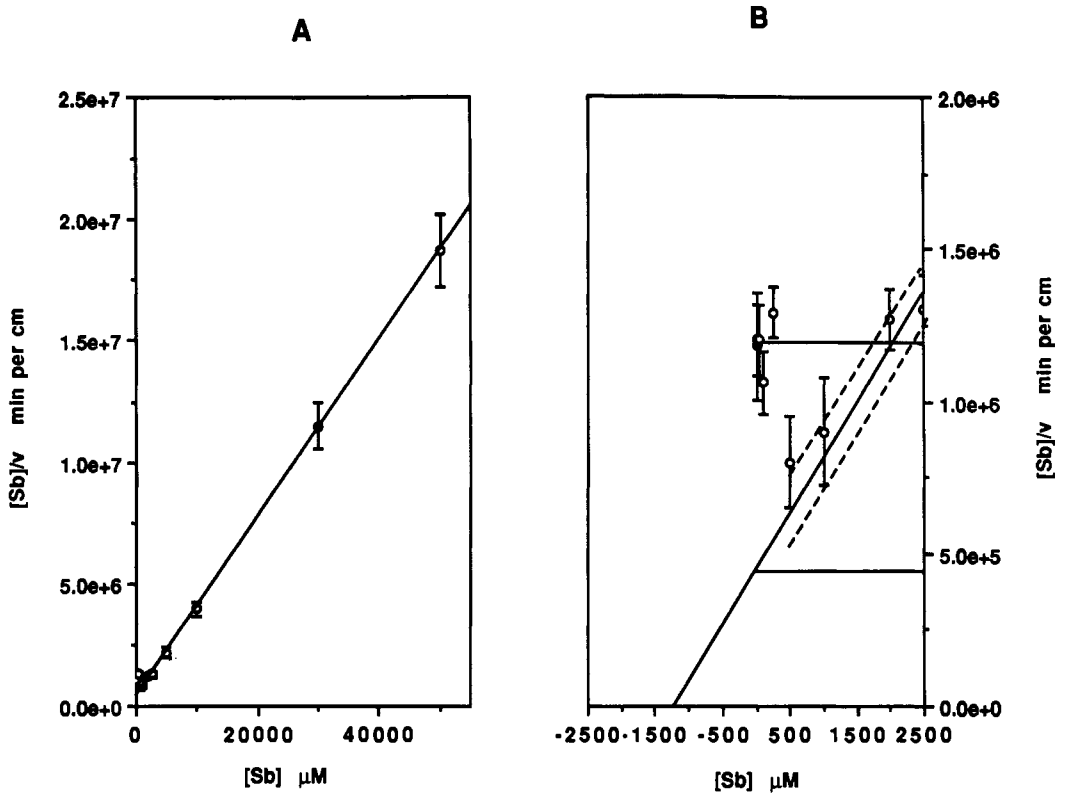

FIGURE 6: Hanes–Woolf plot of zero-trans 3OMG exit data. Zero-trans exit was measured over the [3OMG$_i$] range 6.7 μM to 50 mM ± 50 μM phloretin. (A) Ordinate: [3OMG]/phloretin-sensitive exit rate in min cm^{-1}. Abscissa: [3OMG$_i$] in μM. Phloretin-insensitive exit (leakabe) was subtracted from total fluxes to obtain "saturable" transport. The obtained fluxes [mol (L of cell water)$^{-1}$ min^{-1}] were converted to mol (cm^2 of cell surface area)$^{-1}$ s^{-1} assuming a red cell water content of 42.75 ± 1.3 fL and a rat erythrocyte surface area of 96 μm^2. The line drawn through the points represents least-squares analysis of the data points at the five highest concentrations of 3OMG$_i$. Data are shown as mean ± SD of two duplicate estimates. (B) Data from (A) with condensed ordinate and abscissa in order to illustrate the deviation of data at low [3OMG] from regression analysis of data at high [3OMG]. The line of best fit computed in (A) is shown with 95% confidence bands for the true mean of y. The lines running parallel to the abscissa indicate the intercept of the regression fit (lower line) and the value on the abscissa at [3OMG$_i$] = 6.7 μM.

μM) from medium containing 1 mM 3OMG (P_2) by rat erythrocytes containing 20 mM 3OMG (P_1) was measured in parallel with the time course of [^{14}C]-3OMG (S_1, 3.2 μM) net exit from cells containing 20 mM 3OMG (P_1) into saline containing [^{14}C]-3OMG (S_2, 0.16 μM) and 1 mM 3OMG (P_2). Figure 7 shows the ratio of S_1/S_2 and the concentration of P_1 observed during the course of the experiments.

Discussion

Rat erythrocyte sugar transport is mediated by two distinct mechanisms. At physiological sugar levels (<10 mM), the largest component of transport is mediated by a saturable, stereoselective mechanism displaying accelerated exchange and inhibition by relatively low concentrations of cytochalasin B and phloretin. These features are characteristic of sugar transport systems found in other cell types (Stein, 1986) and suggest that a limited number of sugar carriers (proteins) catalyze the rapid transmembrane flux of monosaccharide. The permeability coefficients [$P_{sat} = V_{max}/K_{m(app)}$] for saturable DG and 3OMG transport at 24 °C are 3.3 × 10^{-9} and 52 × 10^{-9} cm s^{-1} (4.4 × 10^{-3} and 69.2 × 10^{-3} min^{-1}), respectively. Assuming 800 carriers per cell (see Materials and Methods), the turnover number of the rat erythrocyte sugar carrier is 16 molecules of DG and 35 molecules of 3OMG per second for saturated zero-trans sugar uptake at room temperature. By comparison, the turnover number of the human erythrocyte carrier (saturated DG uptake at room temperature) is 60–120 molecules of DG per second.

The second component of rat RBC transport (that component persisting in the presence of high concentrations of the transport inhibitors cytochalasin B and phloretin) is not saturable over the range of sugar concentrations employed (0.007–50 mM). This component of transport could be mediated via trans-bilayer passive diffusion ("leakage") of sugar. The permeability coefficients for leakage (P_1, 6 × 10^{-10} and 3 × 10^{-10} cm s^{-1} for DG and 3OMG, respectively, at 24 °C) are very close to those measured for DG leakage across protein-free egg lecithin vesicles at this temperature (7 × 10^{-10} cm s^{-1}; Carruthers & Melchior, 1983b). Trans-bilayer diffusion of molecules is believed to involve two key processes—partitioning of the molecule between the bilayer hydrocarbon core and the extramembranous aqueous phase plus the non-Stokesian diffusion of the molecule within the hydrocarbon bilayer core (Lieb & Stein, 1986). While the data are not available, it is expected that the solubility of 3OMG in the bilayer hydrocarbon core would be somewhat greater than that of DG, owing to the presence of an additional methyl group at carbon 3. However, non-Stokesian diffusion of molecules within the hydrocarbon core of the bilayer of human red cell membranes is characterized by a steeply exponential relationship between the resistance to diffusion and diffusant molecular mass [see Figure 2.16 of Lieb and Stein (1986)]. This could account for the lower transbilayer permeability coefficient for the larger molecule, 3OMG.

The rat erythrocyte has been assumed to lack protein-mediated hexose transport. This view is based upon a reported lack of measurable transport activity (Rosenburg et al., 1956) or immunoreactivity with antisera raised against the human red cell sugar transport protein (Sogin & Hinkle, 1980a). Figures 1–7 demonstrate that by all the criteria established

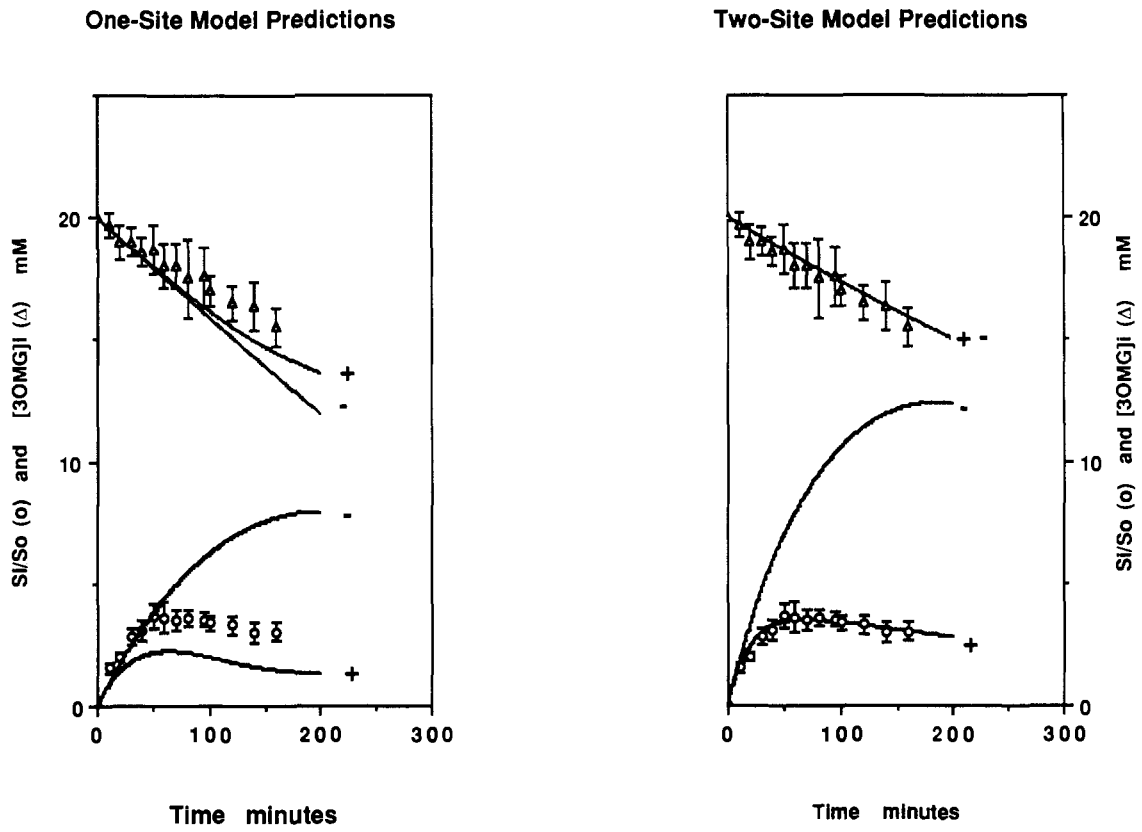

FIGURE 7: Counterflow procedure. Uptake of [^{14}C]-3OMG (3.2 μM, O) from medium containing 1 mM unlabeled 3OMG by cells loaded with 20 mM unlabeled 3OMG. Also shown in the time course of net loss of intracellular 3OMG (Δ) into 1 mM 3OMG. This part of the experiment was performed by loading cells with 20 mM 3OMG plus 3.2 μM [^{14}C]-3OMG. The cells were then collected, the supernatant was diluted 20-fold, and the cells were resuspended in diluted supernatant (100 volumes of supernatant to cells). Equilibrium time points for both label uptake and label net exit were obtained by overnight incubation. These points were then used to calculate the ratio of $label_i$ to $label_o$ (Si/S_o) for the uptake experiment. The time course data shown in both panels represent the same data set (the mean ± SD of five separate duplicate estimates). Predictions of the one-site carrier model are shown in the left panel, and predictions of the two-site model are shown to the right. Predicted results (shown by the curves) were calculated for two conditions. The first represents a situation in which cells contain a single homogeneous intracellular water/sugar pool [indicated by the (−) sign]. The second represents cells containing a subplasmalemmal, intracellular unstirred sugar layer [indicated by the (+) sign]. In this latter case we employed a rate constant (D_1) of 0.01 min^{-1} for sugar flux across this barrier and assigned the subplasmalemmal sugar compartment a volume of 0.25 isotonic cell volume.

for other hexose transfer systems (sugar-displaceable cytochalasin B binding, cytochalasin B and phloretin inhibitable, saturable transport, and accelerated exchange transport), the rat erythrocyte contains significant hexose transfer capacity. As with human erythrocyte DG transport (Stein, 1986), phloretin and cytochalasin B compete with sugar for binding to the influx and efflux sites, respectively, of the rat erythrocytes sugar transport system. Comparison with the human red cell hexose transfer system (Jung & Rampall, 1977; Helgerson & Carruthers, 1987) indicates that the rat erythrocyte contains some 190–380-fold fewer DG-inhibitable cytochalasin B binding (sugar carrier) proteins.

Mechanisms of Transport. We now consider an analysis of catalytic mechanisms for saturable 3OMG transport in rat erythrocytes. We evaluate the ability of two fundamentally different theoretical models for transport to simulate our experimental data. The *one-site carrier* describes a transport mechanism in which sugar influx and efflux substrate binding sites are mutually exclusive. The *two-site carrier* describes a transport mechanism in which sugar influx and efflux substrate binding sites can exist simultaneously but may interact in a cooperative fashion when occupied by substrate.

(A) Analysis of Steady-State (Initial Rate) Transport Data. The steady-state solution to the one-site (alternating conformer) carrier model for transport of a single sugar species (Widdas, 1952) can be reduced to four independent parameters [three independent and one dependent resistance (R) terms and a single affinity (K) term (Stein, 1986)], each being determined from the $K_{m(app)}$ and V_{max} parameters measured in the various transport experiments (Table II). These resistance and affinity parameters have been calculated for rat erythrocyte 3OMG transport (Table III). The one-site model predicts only one K (affinity) parameter for transport of a single sugar species, but three are measured experimentally. This finding represents sufficient grounds for rejection of the one-site carrier. In addition, we compute tests of the one-site carrier mechanism in Table III as described in Stein (1986). Failure of any of these tests represents sufficient grounds for rejection of the one-site carrier. Three out of four of these tests result in failure of the one-site model.

The two-site transport model (which assumed five independent parameters) is more successful in mimicking the steady-state experimental rat RBC transport data (Table IV). Our analysis indicates values of unity for the cooperativity factor (α) and the asymmetry factor (λ). Thus only three parameters (K, V, and V^{ce}) are needed to model the experimental data.

While these findings strongly suggest that predictions of the one-site carrier model are inconsistent with the operational characteristics of red cell sugar transport, statistical variation may be sufficient to account for any discrepancies between theoretical and experimental data. For example, predicted one-site $K_{m(app)}$ for zero-trans 3OMG exit range from 0.29 ± 0.03 to 0.95 ± 0.07 mM. The measured parameter is 0.94

Table III: Analysis of Erythrocyte Transport Data Assuming a One-Site Carrier System[a]

	sugar	
	3OMG	DG
R_{21}[b]	(1.546 ± 0.054) × 10^4	(3.33 ± 0.21) × 10^4
R_{12}[b]	(1.558 ± 0.039) × 10^4	
R_{oe}[b]	(0.259 ± 0.007) × 10^4	(0.268 ± 0.006) × 10^4[d] (R_{oe}^{sp})[b]
R_{oo}[b]	(2.845 ± 0.100) × 10^4	
K[c]		
K_{12}^{zt}	0.515 ± 0.037	
K_{21}^{zt}	0.489 ± 0.038	7.99 ± 0.47
K^{oe}	0.228 ± 0.009[e]	
K_{12}^{ic}	0.179 ± 0.024[e]	
counterflow	5.6 ± 1.3[e]	

Tests[f]

(1) $A = \frac{K_{12}^{zt}}{K_{21}^{zt}} = \frac{V_{12}^{zt}}{V_{21}^{zt}} \rightarrow A = 1.02 \pm 0.11$

(2) $A + 1 = \frac{K^{oe}}{K_{12}^{ic}} + \frac{K_{12}^{zt}}{K^{oe}} \rightarrow 2.02 \pm 0.11 = 3.12 \bullet 0.41$ reject[g]

(3) $(A + 1)^2 \geq 4\frac{K_{12}^{zt}}{K_{12}^{ic}} \rightarrow 4.08 \pm 0.46 = 4.13 \pm 0.27$ accept[g]

(4) $\frac{V_{12}^{zt}}{K_{12}^{zt}} = \frac{V_{21}^{zt}}{K_{21}^{zt}} = \frac{V^{oe}}{K^{oe}} \rightarrow 68.3 \pm 6.5 = 71.9 \pm 8.7 = 154 \pm 9$ reject[g]

(5) $\frac{1}{K_{12}^{zt}} + \frac{1}{K_{21}^{zt}} = \frac{K^{oe}}{K_{12}^{zt}K_{12}^{ic}} \rightarrow 2.17 \bullet 0.17 = 2.92 \pm 0.12$ reject[g]

[a] K can be calculated from any of the four available Michaelis parameters for transport provided the appropriate resistance parameters are known. K was also calculated from the counterflow transient data. Results are shown as mean ± 1 SD. [b] In min/M. [c] In mM. [d] Heteroexchange 3OMG exit by cells containing saturating 3OMG into medium containing variable [DG_o]. [e] The difference between K parameters estimated here and K parameters obtained from transport measurements made under zero-trans conditions is significant at the $p < 0.01$ level (two-tailed t test). [f] These tests or constraints are described in Stein (1986) and must all hold true for acceptance of the one-site carrier mechanism. [g] Indicates whether the tests are satisfied.

± 0.06 mM. Our analyses indicate that the lower estimate of $K_{m(app)}$ is significantly different from the measured value, but it is possible that experimental and biologic variation amplified by analytical procedures with their inherent assumptions could account for these differences. A more sensitive test using reliable statistical methods for analysis would be helpful in confirming the hypothesis that the predictions of the one-site carrier are inconsistent with the experimental data.

One such test is the heteroexchange unidirectional infinite-cis 3OMG exit experiment (Figure 5) in which saturated 3OMG exit (exit at 50 mM $3OMG_i$, internal sites 98% saturated with sugar) is measured at varying [DG_o]. The one-site carrier resistance and affinity terms needed to predict the outcome of this type of experiment have been determined experimentally (Table III); thus, no assumptions or extrapolations are required to calculate one-site carrier predictions for heteroexchange. We performed linear regression analysis on Hanes–Woolf, linear transformations of one- and two-site transport predictions and experimental data in which the x variable was [DG] and the y variable was [DG]/($v^{sp} - v_{12}^{szt}$), where $v^{sp} - v_{12}^{szt}$ represents the increase in 3OMG (S) exit produced by extracellular DG (P) above saturated exit seen in the absence of DG (v_{12}^{szt}). This permits t tests of hypothesis about the mean values for y variables (μ). The computed 95% confidence intervals for the mean y variable (μ) for the experimental data set are $\mu_l = 95.5 < \mu = 96.6 < \mu_h = 98.5$ min. The corresponding values for the one-site carrier are $\mu_l = 224.5 < \mu = 234 < \mu_h = 243.5$ min and for the two-site carrier are $\mu_l = 83.7 < \mu = 91.2 < \mu_h = 98.7$ min. The probability (t test) that $\mu_{2\text{-site}} = \mu_{data} > 95\%$ while the probability that $\mu_{1\text{-site}} = \mu_{data} < 0.5\%$. This analysis does not prove that transport is mediated by a two-site mechanism but does provide sufficient grounds for rejection of the one-site transport mechanism.

(*B*) *Analysis of Counterflow Data.* At the peak of the counterflow transient, radiolabeled sugar uptake and exit are identical. At this point the affinity constant for transport via a one-site carrier (K) can be estimated from measurements of total intracellular sugar (P_1) and the ratio of intracellular to extracellular label (S_1/S_2—see eq 3). Table III indicates that estimates of K obtained from counterflow experiments are much greater than those obtained with steady-state transport data. In addition, the ratio of intracellular to extracellular radiolabeled 3OMG observed at the counterflow peak is lower (2.5-fold) than that predicted by the one-site

Table IV: Analysis of Erythrocyte Transport Data Assuming a Two-Site Carrier Mechanism[a]

	sugar	
	3OMG	DG
λ	1.02 ± 0.11	
α	1.09 ± 0.25	1.25 ± 0.27[b]
β	5.84 ± 0.32	12.4 ± 1.5[b]
K[c]	0.95 ± 0.08	6.8 ± 0.4
V[d]	64.5 ± 2.0	30.0 ± 2.0

	measured		predicted	
procedure	$K_{m(app)}$[c]	V_{max}[d]	$K_{m(app)}$[c]	V_{max}[d]
zero-trans entry	0.90 ± 0.07	64.7 ± 2.2	0.95 ± 0.08	64.5 ± 2
zero-trans exit	0.94 ± 0.06	64.2 ± 1.6	0.95 ± 0.08	64.5 ± 2
equilibrium exchange[e]	K = 1.08 ± 0.11	V = 66.1 ± 1.9	K = 0.95 ± 0.08	V = 64.5 ± 2
	$K_{0.5}$ = 2.2 ± 0.2[f]	β = 5.7 ± 0.2	$K_{0.5}$ = 2.02 ± 0.15[f]	β = 5.84 ± 0.32
infinite-cis net exit	0.91 ± 0.08	65.5 ± 4	1.04 ± 0.23	64.5 ± 2
unidirectional inifinite-cis exit	1.1 ± 0.2	379 ± 11	1.04 ± 0.23	377 ± 20
	8.5 ± 1.2[b]	373 ± 9[b]	8.5 ± 1.8[b]	372 ± 45[b]
unidirectional inifinite-cis entry	0.9 ± 0.1	366 ± 15	1.04 ± 0.23	377 ± 20

[a] Results are shown as mean ± 1 SD. [b] Heteroexchange condition (external D-glucose stimulation of saturated 3OMG exit). [c] In mM. [d] In μmol L^{-1} min^{-1}. [e] Equilibrium exchange [substrate] velocity data were directly fitted to eq 10 according to the Marquardt–Levenberg procedure to obtain estimates of K, V, and β. Pooling the entire equilibrium exchange data set (n = 58), averaging v^{oe} at each [3OMG] (n = 7), and weighting the analysis by the calculated SD for v^{oe} at each [3OMG], χ^2 for the two-site fit (a measure of the discrepancy between observed and predicted transport rates) is 1.25, thus, there is a less than 2.5% statistical probability that the observed values deviate from the predicted values. [f] $K_{0.5}$ (that concentration of sugar at which the rate of transport is $0.5V_{max}$) was predicted with eq 11 and measured experimentally as in Table II.

model. λ (the asymmetry factor) for the two-site model can be obtained directly from the counterflow transient peak with eq 6. Using our experimental findings, we calculate λ is 25.7 ± 3.9. Measurements of V_{max} for entry and exit in rat RBCs indicate an equality in velocity parameters; i.e., $\lambda = 1$. The ratio of intracellular to extracellular radiolabeled 3OMG observed at the counterflow peak is lower (3.5-fold) than that predicted by the two-site model.

One possible explanation for these observations is that leakage of sugar across the bilayer ($k_l = 0.0004$ min^{-1}) invalidates the use of eq 2 and 3. This seems unlikely because at the peak of the counterflow transient leakage-mediated transport of label accounts for no more than 0.1% and 1.5% of total uptake and exit, respectively.

Miller (1968) and Naftalin et al. (1985) have suggested that compartmentalization of intracellular sugars by red cells could give rise to a complex counterflow kinetic. Our studies demonstrate that rat erythrocytes may indeed contain an intracellular unstirred layer. This is an important finding because exchange of sugar between an unstirred sugar layer below the plasma membrane and bulk cellular sugar could be rate limiting for transport under conditions where the sugar concentration of the subplasmalemmal compartment falls below (in exit experiments) or exceeds (in uptake experiments) the bulk intracellular compartment sugar concentration. This could explain why predicted time courses of glucose exit from human red cells using estimates of $K_{m(app)}$ and V_{max} obtained by rapid-quenching procedures are more rapid than experimental time courses (Naftalin et al., 1985) and why $K_{m(app)}$ for exit obtained by integration of the time course of glucose efflux increases with increasing loading glucose concentrations (Naftalin et al., 1985). Equilibrium exchange transport determinations are unaffected by compartmentalization (Lieb & Stein, 1974) because the specific activity of sugar in the extracellular and intracellular compartments is identical.

Figure 7 summarizes simulations of rat erythrocyte counterflow experiments. We have examined the predictions of both one- and two-site carrier models (using one-site K and resistance parameters and two-site K, V, and V^{ee} parameters calculated from initial rate data), allowing for transmembrane leakage of sugar (K_L) and the possibility of an intracellular permeability barrier between the plasma membrane and bulk intracellular solutions. In order to mimic the experimental data with the two-site model, we employed an unstirred layer characterized by a permeability coefficient for 3OMG (D_l) of 0.01 min^{-1} and intracellular bulk solution and subplasmalemmal solution compartments (C_l^b and C_l^m, respectively) of unequal, isotonic volume ($C_l^m/C_l^b = 1/3$).

The value of D_l employed in these simulations is 2.5-fold lower than the apparent value measured. These simulations are arbitrary—they do not indicate whether this is a discreet solution, and they employ hypothetical compartments of undetermined but assumed volume. However, they illustrate the point that slow sugar exchange between intracellular compartments can result in underestimation of transport rates when the duration of transport measurement permits significant deviations between sugar concentrations in C_l^m and C_l^b. While our simulations confirm that the accuracy of zero-trans and infinite-cis initial rate determinations in this study is unaffected by this problem owing to the short incubation periods employed, such considerations indicate that inaccuracies in initial rate transport determinations in the human red cell (a cell with 500–3000-fold greater sugar transport capacity) would be exacerbated by this problem. These findings are consistent with Naftalin's hypothesis (1985) that sugars are compartmentalized in red cells due to nonspecific complexation with hemoglobin.

General. This study was initiated to test the ability of two quite different theoretical mechanisms to predict the sugar transport characteristics of rat erythrocytes. While only one of these models (the two-site model) successfully mimics the steady-state (initial rate) transport properties of rat erythrocytes, we were forced to invoke the notion of compartmentalization of intracellular sugar in order to mimic the counterflow experiments. Studies of human red cell sugar transport also support this view (Miller, 1968; Naftalin & Holman, 1977; Naftalin et al., 1985).

Previous studies (Lowe & Walmsley, 1986; Wheeler, 1986) have suggested that the one-site model provides an adequate description of DG transport in human RBCs at 0–2 and at 20 °C. This current study demonstrates that this is not the case for 3OMG transport in rat erythrocytes. Stein (1986) summarizes criteria for accepting the one-site model (see Table III, tests 1 and 2). Using the human red cell glucose transport data reported by Lowe and Walmsley (1986) and Wheeler (1986) and those reported in Baker and Naftalin (1979) and Sen and Widdas (1962), which are confirmed in Lacko et al. (1972), we calculate

test 1

at 20 °C $A = 3.1 \pm 0.1$

at 0 °C $A = 12.75 \pm 0.93$

test 2

at 20 °C $A + 1 = 10.39 \pm 1.2$; hence, $A = 9.39 \pm 1.2$

at 0 °C $A + 1 = 33.67 \pm 3.33$; hence, $A = 32.67 \pm 3.33$

Testing the null hypothesis that $A = (A + 1) - 1$ at 0 and 20 °C, we are forced to reject this hypothesis at both temperatures ($p < 0.01$). This represents sufficient grounds for rejection of the one-site carrier model for human erythrocyte DG sugar transport. The experimental inconsistency with the one-site carrier model results from the low $K_{m(app)}$ for infinite-cis DG net exit relative to $K_{m(app)}$ for exchange.

In the zero-trans efflux study by Wheeler (1986), 10 volumes of glucose-loaded cells (33% Ht in glucose solution containing labeled sugar) were injected into 1000 volumes of glucose-free medium. This means that the extracellular labeled glucose content of the cell suspension is diluted 152-fold. This has a serious result on efflux determinations. If cells are loaded with 16 mM glucose (one of the [DG] employed by Wheeler (1986)), the extracellular concentration of glucose at zero time is 0.105 mM. Given an estimated $K_{m(app)}$ for glucose influx of 0.17 mM (Wheeler, 1986), the extracellular sites are 38% saturated with glucose at an identical specific activity with that inside the cell. Thus exit is underestimated by 38%. These technical problems invalidate the conclusions of Wheeler's (1986) study. We avoided this problem by mixing 10 mL of sugar-free medium with cell suspensions (10 μL at 80% Ht in 3OMG plus labeled sugar). At the highest [$3OMG_i$] employed in this study (50 mM for zero-trans exits), the zero-time [$3OMG_o$] is never greater than 10 μM, and thus, the extracellular sites are never more than 1% saturated with sugar.

Lowe and Walmsley (1987) have performed rapid-quench studies of pre-steady-state DG uptake. Their strategy was to use extracellular maltose to trap one-site carrier in the X_2 configuration. The system was then perturbed by dilution of

extracellular maltose and addition of low [DG], and a surge of glucose uptake was measured which rapidly decayed within 20 ms. Lowe and Walmsley (1987) interpret their findings to measure the turnover of the one-site carrier. Naftalin (1988) shows that this conclusion is based upon invalid analytical assumptions and that the data are, in fact, *inconsistent* with the one-site carrier model for sugar transport. Naftalin (1988) proposes a fixed (two-site) model consistent with the findings of Lowe and Walmsley (1987) in which dissociation of maltose from the external sugar binding site cycles the binding site through a slowly relaxing high-affinity state. This hypothesis could account for the data of Appleman and Lienhard (1985), demonstrating that DG increases the apparent rate constant for ethylideneglycose- (EG) induced quenching of carrier intrinsic fluorescence.

General Conclusions. The basic tenet of the kinetic approach is to utilize the simplest model capable of quantitatively predicting the experimental data. It is often assumed that the one-site carrier model is more rudimentary than the two-site model for transport (Stein, 1986; Lowe & Walmsley, 1986; Wheeler, 1986). In this study we find that the steady-state transport properties of rat erythrocyte sugar transport can be modeled successfully by the two-site carrier mechanism. We assumed rapid equilibrium kinetics in order to simplify the derivation of the two-site carrier transport equations. As transport of 3-*O*-methylglucose is symmetric with no indication of cooperativity (i.e., λ and α are unity), it is possible to characterize the two-site carrier transport equations by only three constants (V, V^{ee}, and K). The success of these equations obviates the formal need to derive the steady-state (non rapid equilibrium) solutions to the two-site model. The one-site carrier transport equations contain four independent constants and are less successful in predicting the transport properties of the rat erythrocyte. Thus in a formal sense, the two-site model is less complex than the one-site model. Previous studies have indicated that both one- and two-site mechanisms can account for the transport properties of nerve and muscle (Baker & Carruthers, 1981, 1984; Carruthers, 1983). In these studies, the one-site carrier equations were characterized by four independent constants whereas the two-site carrier equations were characterized by three (Carruthers, 1983) or four (Baker & Carruthers, 1981, 1984). Were we to accept the view that the simplest model for transport should be accepted over more complex models, we would be forced to accept the two-site model for transport in these instances.

It should be emphasized that while the success of a theoretical model for transport does not confirm that transport is mediated by such a theoretical mechanism, the failure of a model represents sufficient grounds for its rejection. This current study supports rejection of the one-site model as an appropriate model for rat erythrocyte sugar transport.

Although studies from other laboratories (Sogin & Hinkle, 1980b; Gorga & Lienhard, 1981) may disagree with this conclusion, our laboratory and others have presented three independent lines of evidence suggesting that mammalian erythrocyte sugar transport is inconsistent with the one-site carrier model for transport. This evidence comes from the following: (1) sugar transport studies with human (Baker & Naftalin, 1979; Carruthers & Melchior, 1983a; Lowe & Walmsley, 1986, 1987; Wheeler, 1986; see considerations above; Naftalin, 1988) and rat (this study) erythrocytes; (2) substrate-induced intrinsic fluorescence quenching of purified human erythrocyte sugar transport protein (Carruthers, 1986a) and alkali-washed human red cell membranes (Carruthers, 1986b); (3) ligand binding studies with human red cell ghosts (Helgerson & Carruthers, 1987).

References

Allard, W. J., & Lienhard, G. E. (1985) *J. Biol. Chem. 260*, 8668–8675.

Appleman, J. R., & Lienhard, G. E. (1985) *J. Biol. Chem. 260*, 4575–4578.

Baker, G. F., & Widdas, W. F. (1973) *J. Physiol. (London) 231*, 143–165.

Baker, G. F., & Naftalin, R. J. (1979) *Biochim. Biophys. Acta 550*, 474–484.

Baker, P. F., & Carruthers, A. (1981) *J. Physiol. (London) 316*, 503–525.

Baker, P. F., & Carruthers, A. (1984) *Curr. Top. Membr. Transp. 22*, 91–130.

Birnbaum, M. J., Haspel, H. C., & Rosen, O. M. (1986) *Proc. Natl. Acad. Sci. U.S.A. 83*, 5784–5788.

Carruthers, A. (1983) *J. Physiol. (London) 336*, 377–396.

Carruthers, A. (1986a) *J. Biol. Chem. 261*, 11028–11037.

Carruthers, A. (1986b) *Biochemistry 25*, 3592–3602.

Carruthers, A., & Melchior, D. L. (1983a) *Biochim. Biophys. Acta 728*, 254–266.

Carruthers, A., & Melchior, D. L. (1983b) *Biochemistry 22*, 5797–5807.

Carruthers, A., & Melchior, D. L. (1984) *Biochemistry 23*, 6901–6911.

Ginsburg, H. (1978) *Biochim. Biophys. Acta 506*, 119–135.

Gorga, F. R., & Lienhard, G. E. (1981) *Biochemistry 20*, 5108–5113.

Helgerson, A. L., & Carruthers, A. (1987) *J. Biol. Chem. 262*, 5464–5475.

Holman, G. D. (1980) *Biochim. Biophys. Acta 599*, 202–213.

James, D. E., Brown, R., Navarro, J., & Pilch, P. F. (1988) *Nature 333*, 183–185.

Jung, C. Y., & Rampal, A. L. (1977) *J. Biol. Chem. 252*, 5456–5463.

Lacko, L., Wittke, B., & Kromphardt, H. (1972) *Eur. J. Biochem. 25*, 447–454.

Lieb, W. R., & Stein, W. D. (1971) *Nature New Biol. 230*, 108–116.

Lieb, W. R., & Stein, W. D. (1974) *Biochim. Biophys. Acta 373*, 178–196.

Lieb, W. R., & Stein, W. D. (1986) in *Transport and Diffusion across Cell Membranes* (Stein, W. D., Ed.) pp 69–112, Academic Press, New York.

Lowe, A. G., & Walmsley, A. R. (1986) *Biochim. Biophys. Acta 857*, 146–154.

Lowe, A. G., & Walmsley, A. R. (1987) *Biochim. Biophys. Acta 903*, 547–550.

Lowry, O. H., Rosebrough, N. J., Farr, A. L., & Randall, R. J. (1951) *J. Biol. Chem. 193*, 265–275.

Marquardt, D. W. (1963) *SIAM J. Appl. Math. 11*, 431–441.

Miller, D. M. (1968) *Biophys. J. 8*, 1329–1338.

Mueckler, M., Caruso, C., Baldwin, S. A., Panico, M., Blench, I., Morris, H. R., Allard, W. J., Lienhard, G. E., & Lodish, H. F. (1985) *Science 229*, 941–945.

Naftalin, R. J. (1988) *Biochim. Biophys. Acta* (in press).

Naftalin, R. J., & Holman, G. D. (1977) in *Membrane Transport in Red Cells* (Ellory, J. C., & Lew, V. L., Eds.) pp 257–300, Academic Press, New York.

Naftalin, R. J., Smith, P. M., & Roselaar, S. E. (1985) *Biochim. Biophys. Acta 820*, 235–249.

Ralston, A., & Rabinowitz, P. (1978) in *A First Course in Numerical Analysis*, Section 8.12, McGraw-Hill, New York.
Regen, D. M., & Tarpley, H. L. (1974) *Biochim. Biophys. Acta 339*, 218-233.
Rosenberg, T., Vestergaard, B., & Wilbrandt, W. (1956) *Helv. Physiol. Pharmacol. Acta 14*, 334-241.
Sen, A. K., & Widdas, W. F. (1962) *J. Physiol. (London) 160*, 392-403.
Sogin, D. C., & Hinkle, P. C. (1980a) *Proc. Natl. Acad. Sci. U.S.A. 77*, 5725-5729.
Sogin, D. C., & Hinkle, P. C. (1980b) *Biochemistry 19*, 5417-5420.
Stein, W. D. (1986) in *Transport and Diffusion across Cell Membranes*, pp 231-306, Academic Press, New York.
Stineman, R. W. (1980) *Creative Comput. July*, 54-57.
Wheeler, T. J. (1986) *Biochim. Biophys. Acta 862*, 387-398.
Widdas, W. F. (1952) *J. Physiol. (London) 118*, 23-39.

In Vitro Characterization of Tissue-Specific Nuclear Proteins Preferentially Bound to the Mouse β-Globin Gene during MEL Cell Terminal Differentiation†

Jean-Claude Lelong,* Grégoire Prevost, Kyong-il Lee, and Michel Crepin
Institut d'Oncologie Cellulaire et Moléculaire Humaine, Université de Paris-Nord, 129 route de Stalingrad, 93000-Bobigny, France

Received July 21, 1988; Revised Manuscript Received January 27, 1989

ABSTRACT: Using DNA restriction fragments of the mouse β-globin gene and other promoter-containing DNA fragments (LTR-MMTV and pBR322) as controls, we have characterized by protein blotting, in extracts of mouse erythroleukemia (MEL) cells, specific nuclear DNA binding proteins with a preferential affinity for the β-globin DNA. Some proteins (110 and 75 kDa) appear in differentiated MEL cells while others (100, 95, and 35 kDa) are present in immature MEL and normal erythroblast cells and bind selectively to the far-upstream region of the gene. These proteins could modulate either positively or negatively the expression of the β-globin gene and maybe, of other genes, during the terminal differentiation of erythroid cells.

Expression of the β-globin gene family in erythroid cells appears to be both tissue specifically determined (Collins et al., 1984; Groudine et al., 1981) and inducible (Ross et al., 1974; Wright et al., 1983). Mouse erythroleukemia (MEL) cells are Friend virus transformed erythroid cells, arrested at the proerythroblast stage of differentiation, that are easy to cultivate and may be induced with a variety of chemicals, including dimethyl sulfoxide (DMSO) (Ross et al., 1974). The accumulation of globin transcripts results from both transcriptional activation of the mouse globin genes and increased relative stability of their mRNAs (Hofer et al., 1982). Therefore, this system is a very suitable model to study the tissue-specific factors that are activated in order to promote the selectivity of transcription, leading to a particular type of terminal phenotypic expression. Cis-acting DNA sequences that control human, murine, and chicken β-globin gene transcription have been analyzed by deletion, point mutation, and chimeric gene constructions, using mainly so far either in vivo assays of transient expression of introduced genes (Charnay et al., 1984, 1985; Dierks et al., 1983; Myers et al., 1986; Chao et al., 1983), in vitro transcription systems (Hofer et al., 1982), or transgenic mice (Kollias et al., 1987). These are usually located at chromatin hypersensitive sites [for a review, see Galson and Housman (1988)]. The function of these control DNA elements in the developmental activation and tissue specificity of β-globin transcription requires the coordinate binding of both general and promoter-specific transcription factors. The binding sites of several such sequence-specific DNA binding proteins have been identified in the 5′ upstream flanking region from −300 to −70 bp, in the intragenic sequences, and in 3′ end of the gene [for a review, see Galson and Housman, (1988)].

Although a promoter-specific transcription factor need not be a sequence-specific DNA binding protein and vice versa, an important approach to the understanding of the tissue-specific regulation of gene expression might be to analyze variations during differentiation of cell- and sequence-specific nuclear DNA binding proteins, probed with cloned fragments of a regulated gene.

Because protein blotting (Bowen et al., 1980) is particularly suitable for a rapid and highly resolutive screening of cell crude extracts, we have used this technique to analyze MEL cell nuclear proteins, which have been tested for (1) preferential binding to a cloned mouse β-globin gene, (2) erythroid cell specificity, and (3) modulation of the DNA binding activity after induction of β-globin expression.

We have characterized several DNA binding proteins which satisfy these criteria and have also described results suggesting that three of them may interact with specific sequences located far upstream and downstream from the transcription start.

Experimental Procedures

Cell Lines. Mouse erythroleukemia cells, clone 707-1-C (from Dr. N. Affara), were grown at 37 °C in a 5% CO_2 atmosphere in Ham's F12 medium containing glutamine, 15% horse serum, penicillin (100 units/mL), and streptomycin (100 μg/mL). Cells were collected at a density of 1.5×10^6/mL

† This work was supported by grants from the Centre National de la Recherche Scientifique, the Ministère de lIndustrie et de la Recherche, the Institut National de la Santé de la Recherche Médicale, the Fondation pour la Recherche Médicale Française, and the Association pour la Recherche sur le Cancer.
* To whom correspondence should be addressed.

0006-2960/89/0428-4594$01.50/0